

## Long Baseline Neutrino Physics with a Muon Storage Ring Neutrino Source

V. Barger<sup>1</sup>, S. Geer<sup>2</sup>, and K. Whisnant<sup>3</sup>

<sup>1</sup>*Department of Physics, University of Wisconsin, Madison, WI 53706, USA*

<sup>2</sup>*Fermi National Accelerator Laboratory, P.O. Box 500, Batavia, IL 60510, USA*

<sup>3</sup>*Department of Physics and Astronomy, Iowa State University, Ames, IA 50011, USA*

We examine the physics capabilities of known flavor neutrino beams from intense muon sources. We find that long-baseline neutrino experiments based on such beams can provide precise measurements of neutrino oscillation mass and mixing parameters. Furthermore, they can test whether the dominant atmospheric neutrino oscillations are  $\nu_\mu \rightarrow \nu_\tau$  and/or  $\nu_\mu \rightarrow \nu_s$ , determine the  $\nu_\mu \rightarrow \nu_e$  content of atmospheric neutrino oscillations, and measure  $\nu_e \rightarrow \nu_\tau$  appearance. Depending on the oscillation parameters, they may be able to detect Earth matter and  $CP$  violation effects and to determine the ordering of some of the mass eigenstates.

14.60.Pq, 13.15.+g, 13.35.Bv, 07.77.Ka

### I. INTRODUCTION

In recent years solar-neutrino and atmospheric-neutrino measurements have provided a growing body of evidence for the existence of neutrino oscillations [1]. The observed solar neutrino deficit [2,3] can be interpreted as evidence for the oscillation of electron neutrinos ( $\nu_e$ ) into neutrinos of a different flavor. The recent atmospheric-neutrino results from the Super-Kamiokande collaboration [4], along with other experiments [5] suggest the oscillation of muon neutrinos ( $\nu_\mu$ ) into neutrinos of a different flavor, which are dominantly either tau neutrinos ( $\nu_\tau$ ) or sterile neutrinos ( $\nu_s$ ). Taken together, these results suggest the mixing of at least three different neutrino types [6–9]. In addition, the LSND collaboration has reported [10] results from  $\mu^+$  decays at rest that could be interpreted as the first evidence for  $\bar{\nu}_\mu \rightarrow \bar{\nu}_e$  oscillations in an accelerator based experiment. LSND has also reported [11] results from measurements of  $\pi^+$  decays in flight that could be the first evidence for  $\nu_\mu \rightarrow \nu_e$  oscillations. If all of the above reported effects survive, then oscillations to a sterile neutrino are required, since there would then be three distinct mass-squared difference ( $\Delta m^2$ ) values [12].

The solar-neutrino, atmospheric-neutrino, and LSND results have generated much interest in future accelerator-based neutrino oscillation experiments. We can anticipate that an extensive experimental program will be needed to firmly establish the existence of neutrino oscillations and to precisely determine all the parameters relevant to the phenomenon. The up-coming accelerator-based experiments [13,14] will firmly ground the existence of neutrino oscillations, and measure some of the associated parameters. Also, reactor experiments will tightly constrain  $\nu_e$  disappearance [15–18]; a sensitivity down to  $10^{-5}$  eV<sup>2</sup> is expected in Kamland. However, precise measurements of neutrino mass-squared differences and the mixing matrix that relates neutrino-flavor eigenstates to neutrino-mass eigenstates will almost certainly require a further generation of experiments exploiting higher intensity and/or higher quality neutrino beams than currently available [19–21]. Other goals of such experiments might be (i) to determine whether the atmospheric neutrino oscillations are  $\nu_\mu \rightarrow \nu_\tau$ ,  $\nu_\mu \rightarrow \nu_s$ , or a mixture of both [22,23], (ii) to detect Earth matter effects on neutrino oscillations [24,25], (iii) when matter effects are present, to determine the ordering of the neutrino mass eigenstates responsible for the oscillation being measured [25–27], and (iv) to detect  $CP$  and  $T$  violation if it exists in the lepton sector [20,28–31].

It has been suggested [19] that higher intensity and higher quality neutrino beams could be made by exploiting the very intense muon sources that are currently being developed as a part of ongoing muon collider [32] feasibility studies. The muons would be accelerated up to the desired energy, and injected into a storage ring consisting of two long straight sections joined together by two arcs. Muons that decay in the straight sections would form neutrino beams consisting of 50%  $\nu_\mu$  and 50%  $\bar{\nu}_e$  if negative muons are stored, and 50%  $\nu_e$  and 50%  $\bar{\nu}_\mu$  if positive muons are stored. A compact muon storage ring neutrino source could be tilted downwards at a large angle to enable neutrino beams to be directed through the Earth. If the muons from a muon collider muon source are accelerated to energies of  $\geq 10$  GeV and injected into a suitable storage ring, it has been shown that the neutrino fluxes are sufficient to detect hundreds of neutrino charged current (CC) interactions per year in a reasonable size detector on the other side of the Earth [19].

The muon storage ring neutrino source idea has led to several recent workshops [33,34]. A number of papers [19,20,35,36] have discussed the physics potential of this new type of neutrino facility. In addition, a preliminary muon storage ring neutrino source design study has been made [37], and further studies are planned. The evolution of the existing accelerator complexes at Fermilab [38,39] and CERN [40] towards a muon collider with a muon storage ring neutrino source has also been considered. Much further work will be required to develop a realistic design before the first muon storage ring neutrino source can be proposed.

In this paper we consider the physics potential of muon storage ring neutrino sources that are being considered in explicit upgrade scenarios for the Fermilab accelerator complex. Two different geometries are considered: (i) a neutrino source at Fermilab pointing toward the Soudan mine in Minnesota ( $L = 732$  km), and (ii) a neutrino source at Fermilab pointing toward the Gran Sasso underground laboratory in Italy (baseline length  $L = 7332$  km).

The paper is organized as follows. In Section II the characteristics of neutrino beams from muon storage ring sources are discussed and the basic oscillation formulas are presented. The role of muon storage ring neutrino sources in exploring the parameters associated with  $\nu_\mu \rightarrow \nu_\tau$  and  $\nu_\mu \rightarrow \nu_s$  oscillations is considered in Section III. Section IV discusses  $\nu_e \rightarrow \nu_\mu$  oscillations, including matter effects and the possibility of detecting  $CP$  violation. In Section V we discuss  $\nu_e \rightarrow \nu_\tau$  oscillations. Finally, a summary is given in Section VI.

## II. NEUTRINO BEAMS FROM A MUON STORAGE RING

The neutrino fluxes and interaction rates at a given location downstream of a muon storage ring neutrino source depend upon the number of stored muons, the beam divergence within the neutrino-beam forming straight section, and the energies and polarization of the decaying muons. In this section we describe the storage ring parameters, discuss the muon decay kinematics, present the calculated neutrino fluxes and interaction rates at  $L = 732$  km and 7332 km, and discuss the matter effects for  $\nu_e \rightarrow \nu_\mu$ ,  $\nu_e \rightarrow \nu_\tau$ , and  $\nu_\mu \rightarrow \nu_s$  oscillations.

### A. Storage ring parameters

A preliminary design study for a muon storage ring neutrino source at Fermilab is described in Ref. [37]. The neutrino source consists of:

- (i) An upgraded high-intensity proton source [38] that cycles at 15 Hz, and delivers 12 bunches per cycle, each containing  $2.5 \times 10^{12}$  protons at 16 GeV.
- (ii) A pion production target, pion collection system, and decay channel. The 16 GeV protons interact in the target to produce per incident proton approximately 0.6 charged pions of each sign captured within the decay channel. At the end of a 50 m long decay channel on average 0.2 muons of each charge are produced for each proton incident on the production target. Hence there would be about  $6 \times 10^{12}$  muons of the desired charge at the end of the decay channel per accelerator cycle, and therefore  $9 \times 10^{20}$  muons per operational year ( $10^7$  secs).
- (iii) A muon cooling channel that captures the muons exiting the decay channel into bunches with rms lengths  $\sigma_z = 1.5$  m, and a normalized transverse emittance  $\epsilon_N \sim 0.017$  m-rad. The cooling channel reduces the emittance to  $\epsilon_N \sim 0.005$  m-rad. At the end of the cooling channel there would be about  $5.4 \times 10^{12}$  muons of the desired charge per accelerator cycle, contained within 12 bunches with rms lengths  $\sigma_z = 2$  m, a mean muon energy of 230 MeV, and an energy spread given by  $\sigma_E/E \sim 0.2$ . Hence, there would be  $8.1 \times 10^{20}$  cooled muons per operational year.

- (iv) An acceleration system that captures the muons from each long bunch exiting the cooling channel into 16 short bunches with  $\sigma_z \sim 0.9$  cm, and accelerates the muons to 10 GeV. About 60% of the muons survive the capture and acceleration stage. Hence, about  $5 \times 10^{20}$  muons are accelerated to 10 GeV per operational year.
- (v) A muon storage ring with two long straight sections. The circumference of the ring is 448 m, and the length of the neutrino beam-forming straight section is 150 m. Hence about 33% of the muon decays contribute to the neutrino beam, and there are  $1.6 \times 10^{20}$  neutrinos and  $1.6 \times 10^{20}$  antineutrinos in the beam per operational year.

Note that in the scenario described above the proton source provides approximately one-third of the beam power of the source required for a muon collider. The fluxes and interaction rates discussed in the following sections should be multiplied by a factor of 3.3 to obtain the results that would correspond to a muon storage ring neutrino source that utilizes the full muon collider muon source.

## B. Fluxes and Interaction Rates

In the muon rest-frame the distribution of muon antineutrinos (neutrinos) from the decay  $\mu^\pm \rightarrow e^\pm + \nu_e$  ( $\bar{\nu}_e$ ) +  $\bar{\nu}_\mu$  ( $\nu_\mu$ ) of polarized muons is given by the expression [41]

$$\frac{d^2 N_{\nu_\mu}}{dx d\Omega} = \frac{2x^2}{4\pi} [(3 - 2x) \mp (1 - 2x) \cos \theta], \quad (1)$$

where  $x \equiv 2E_\nu/m_\mu$ ,  $\theta$  is the angle between the neutrino momentum vector and the muon spin direction, and  $m_\mu$  is the muon rest mass. The corresponding expression describing the distribution of electron neutrinos (antineutrinos) is

$$\frac{d^2 N_{\nu_e}}{dx d\Omega} = \frac{12x^2}{4\pi} [(1 - x) \mp (1 - x) \cos \theta]. \quad (2)$$

Thus, the neutrino and antineutrino energy- and angular- distributions depend upon the parent muon energy, the decay angle, and the direction of the muon spin vector. For an ensemble of muons we must average over the polarization of the initial state muons, and the distributions become

$$\frac{d^2 N_{\nu_\mu}}{dx d\Omega} \propto \frac{2x^2}{4\pi} [(3 - 2x) \mp (1 - 2x) P_\mu \cos \theta], \quad (3)$$

and

$$\frac{d^2 N_{\nu_e}}{dx d\Omega} \propto \frac{12x^2}{4\pi} [(1 - x) \mp (1 - x) P_\mu \cos \theta], \quad (4)$$

where  $P_\mu$  is the average muon polarization along the chosen quantization axis, which in this case is the beam direction.

Using Eqs. 3 and 4, the calculated  $\nu_\mu$ ,  $\nu_e$ ,  $\bar{\nu}_\mu$ , and  $\bar{\nu}_e$  fluxes at a muon storage ring neutrino source were presented in Ref. [19] as a function of  $L$ ,  $P_\mu$ , and the energy of the stored muons ( $E_\mu$ ). For unpolarized muons, these results can be summarized by the formula

$$\Phi \equiv \frac{d^2 N_\nu}{dA dt} = \frac{n_0}{4\pi L^2 \gamma^2 (1 - \beta \cos \alpha)^2}, \quad (5)$$

where  $n_0$  is the number of neutrinos (or antineutrinos) per unit time in a given beam,  $\gamma = E_\mu/m_\mu$ ,  $\beta = p_\mu/E_\mu$ ,  $\alpha$  is the angle between the beam axis and the direction of interest, and  $dA$  is the differential area at the detector. In practice the muon beam within the storage ring will have a finite divergence which must be taken into account. Current design studies suggest a typical divergence of  $\sim 1$  mr within the beam-forming straight section. The neutrino flux at  $L = 732$  km is shown versus  $\alpha$  in Fig. 1 for several muon energies. In Fig. 2 the neutrino flux is shown versus the perpendicular distance from the beam axis for several values of  $L$  and  $E_\mu$ . As Fig. 2 shows, the flux is fairly uniform near the axis, and, provided  $1/\gamma > 1$  mr, begins to fall off only for distances of order  $L/\gamma$  away from the beam. In the extreme forward direction  $\cos \alpha \simeq 1$ , and using the approximation  $\beta \simeq 1 - 1/(2\gamma^2)$ , the neutrino flux may be approximated as

$$\Phi \simeq \frac{n_0 \gamma^2}{\pi L^2}. \quad (6)$$

These calculated fluxes are summarized in Table I for the baseline lengths  $L = 732$  km and  $L = 7332$  km, and the storage ring parameters described Section II.A.

Equations 3 and 4 can also be used to calculate the distribution  $dN_\nu/dE_\nu$  of  $\nu_\mu$  and  $\nu_e$  energies in the beam using the approximation that, in the laboratory frame,  $x \rightarrow E_\nu/E_\mu$  for forward neutrinos from high energy muon decays ( $E_\mu \gg m_\mu$ ). The calculated  $\nu_\mu$  and  $\nu_e$  spectra are shown in Fig. 3. Note that the  $\nu_\mu$  spectrum peaks at the stored muon beam energy, whereas the  $\nu_e$  spectrum peaks at two-thirds of the stored muon beam energy. Also, since  $\Phi \propto E_\mu^2$  and  $\sigma \propto E_\mu$ , the total event rate is proportional to  $E_\mu^3$ .

The CC neutrino and antineutrino interaction rates can be calculated using the approximate expressions for the cross sections

$$\sigma_{\nu N} \sim 0.67 \times 10^{-38} \text{ cm}^2 \times E_\nu \text{ (GeV)} \quad (7)$$

and

$$\sigma_{\bar{\nu} N} \sim 0.34 \times 10^{-38} \text{ cm}^2 \times E_{\bar{\nu}} \text{ (GeV)}. \quad (8)$$

The modification in the linear energy dependence due to the  $W$  propagator can be neglected for the neutrino energies we consider. Using Eqs. 7 and 8, and assuming no neutrino oscillations, the CC interaction rates corresponding to the fluxes in Table I are shown in Table II. Given the distribution of neutrino and antineutrino energies in the beam (Fig. 3), and the linear dependence of the CC cross sections with energy (Eqs 7 and 8), the predicted energy distributions for the resulting CC interactions are shown in Fig. 4. Note that the  $\nu_\mu$  CC event energies peak at the stored muon beam energy, whereas the  $\nu_e$  event energies peak at about three-quarters of the stored muon beam energy. For  $\nu_\tau$  and  $\bar{\nu}_\tau$  CC cross sections, we use the ratios  $\sigma_{CC}(\nu_\tau N)/\sigma_{CC}(\nu_\mu N)$  and  $\sigma_{CC}(\bar{\nu}_\tau N)/\sigma_{CC}(\bar{\nu}_\mu N)$  given in Ref. [42], multiplied by the cross sections in Eqs. 7 and 8. If the  $\nu_\tau$  cross sections from Ref. [43] are used, the predicted event rates are 20–30% higher; we use the more conservative values of Ref. [42].

Event rates for MINOS are compared to those for a Fermilab to Soudan experiment using a muon storage ring in Table III. Since for a muon storage ring neutrino source the total event rate increases as  $E_\mu^3$ , increasing the muon energy dramatically improves the usefulness of such a machine. From this comparison we conclude: (i) for electron neutrino beams, even a very low energy muon storage ring might be interesting, and (ii) for muon neutrino beams, rates become quite large compared to conventional neutrino beams for  $E_\mu \geq 20$  GeV.

We next consider the distribution of energies of the charged leptons produced in the neutrino and antineutrino CC interactions downstream of a muon storage ring neutrino source. It is useful to define the scaling variable

$$y \equiv 1 - E_l/E_\nu, \quad (9)$$

where  $E_l$  is the energy of a charged lepton produced the CC interaction. The differential neutrino and antineutrino cross sections are given approximately by

$$\frac{d\sigma_\nu}{dy} \propto E_\nu \left[ 1 + \frac{(1-y)^2}{5} \right], \quad (10)$$

and

$$\frac{d\sigma_{\bar{\nu}}}{dy} \propto E_{\bar{\nu}} \left[ (1-y)^2 + \frac{1}{5} \right]. \quad (11)$$

These formulas neglect the  $Q^2$  dependence of the structure functions. If *unpolarized* positive muons are stored in the muon storage ring neutrino source, the  $\bar{\nu}_\mu$  CC interaction rate in a distant detector is described by the doubly differential distribution obtained from Eqs. 1 and 11

$$\frac{d^2 N_{\bar{\nu}_\mu}^{CC}}{dx dy} \propto x^3 (3 - 2x) \left[ (1-y)^2 + \frac{1}{5} \right], \quad (12)$$

where, for a high energy muon storage ring,  $x \rightarrow E_\nu/E_\mu$  in the laboratory frame. It is convenient to define the normalized charged lepton energy

$$z \equiv E_l/E_\mu. \quad (13)$$

At high energies  $(1-y) \simeq z/x$ . Integrating Eq. 12 over  $x$ , the charged lepton energy spectrum is given by

$$\frac{dN_{\mu^+}}{dz} \propto \int_z^1 dx x^2(3-2x) \left[ \left(\frac{z}{x}\right)^2 + \frac{1}{5} \right], \quad (14)$$

yielding

$$\frac{dN_{\mu^+}}{dz} \propto 1 + 20z^2 - 32z^3 + 11z^4. \quad (15)$$

The corresponding expression for the electron energy spectrum arising from the CC  $\nu_e$  interactions is

$$\frac{dN_{e^-}}{dz} \propto 5 + 6z^2 - 32z^3 + 21z^4. \quad (16)$$

The expressions for the  $\mu^-$  and  $e^+$  spectra resulting from CC interactions when unpolarized negative muons are stored in the muon storage ring neutrino source are respectively

$$\frac{dN_{\mu^-}}{dz} \propto 5 + 4z^2 - 16z^3 + 7z^4, \quad (17)$$

and

$$\frac{dN_{e^+}}{dz} \propto 1 + 30z^2 - 64z^3 + 33z^4. \quad (18)$$

The charged lepton spectra computed from Eqs. 15–18 are shown in Fig. 5.

### C. Interaction Rates with Neutrino Oscillations

For a given neutrino flavor, neutrino oscillations will modify the neutrino flux at a distant detector, and hence the associated charged current interaction rates. Within the framework of two-flavor vacuum oscillations, the flavor eigenstates  $\nu_\alpha$  and  $\nu_\beta$  are related to the mass eigenstates  $\nu_i$  and  $\nu_j$  by

$$\nu_\alpha = \nu_i \cos \theta - \nu_j \sin \theta, \quad (19)$$

$$\nu_\beta = \nu_i \sin \theta + \nu_j \cos \theta, \quad (20)$$

where  $\theta$  is the mixing angle. The probability that, while traversing a distance  $L$  in vacuum, a neutrino of type  $\alpha$  oscillates into a neutrino of type  $\beta$  is given by

$$P(\nu_\alpha \rightarrow \nu_\beta) = \sin^2(2\theta) \sin^2(1.267 \Delta m_{ji}^2 L / E_\nu), \quad (21)$$

where  $\Delta m_{ji}^2 \equiv m_j^2 - m_i^2$  is measured in  $\text{eV}^2/c^4$ ,  $L$  in km, and the neutrino energy  $E_\nu$  is in GeV. The neutrino oscillation length in vacuum  $L_V$  is given by

$$L_V = \frac{2.48 E_\nu}{\Delta m_{ji}^2}. \quad (22)$$

The first maximum in the oscillation probability occurs when  $L = L_V/2$ . The values of  $\Delta m_{ji}^2$  that correspond to this oscillation maximum are shown in Fig. 6 as a function of  $E_\nu$  for three baseline lengths. Note that if  $\Delta m_{ji}^2$  is small, short baseline lengths require low neutrino energies to probe the oscillation maximum. It is useful to define

$$\eta \equiv \frac{\Delta m_{ji}^2 L}{E_\mu} = \frac{\Delta m_{ji}^2 L}{E_\nu} x. \quad (23)$$

The first maximum in the oscillation probability occurs when  $\eta = 1.24x$ . The modulation of the  $\nu_e$  and  $\nu_\mu$  CC interaction spectra for neutrinos originating from a muon storage ring neutrino source is shown in Fig. 7 as a function of  $\eta$ . The distributions of the  $\nu_\alpha$  CC interaction energies exhibit peaks whose locations are very sensitive to  $\eta$  (and hence  $\Delta m_{ji}^2$ ) provided  $\eta \sim 1$ .

If there are three neutrino types, then the flavor eigenstates are related to the mass eigenstates by a  $3 \times 3$  unitary matrix [44]

$$\begin{pmatrix} \nu_e \\ \nu_\mu \\ \nu_\tau \end{pmatrix} = \begin{pmatrix} c_{12}c_{13} & s_{12}c_{13} & s_{13}e^{-i\delta} \\ -s_{12}c_{23} - c_{12}s_{23}s_{13}e^{i\delta} & c_{12}c_{23} - s_{12}s_{23}s_{13}e^{i\delta} & s_{23}c_{13} \\ s_{12}s_{23} - c_{12}c_{23}s_{13}e^{i\delta} & -c_{12}s_{23} - s_{12}c_{23}s_{13}e^{i\delta} & c_{23}c_{13} \end{pmatrix} \begin{pmatrix} \nu_1 \\ \nu_2 \\ \nu_3 \end{pmatrix}, \quad (24)$$

where  $c_{ij} = \cos \theta_{ij}$  and  $s_{ij} = \sin \theta_{ij}$ . If the neutrinos are Majorana, there are two extra phases, but these do not affect oscillations [45]. If  $\Delta m_{21}^2$  is responsible for solar neutrino oscillations and  $\Delta m_{32}^2$  for atmospheric neutrino oscillations, then  $|\Delta m_{21}^2| \ll |\Delta m_{32}^2|$ . The resulting vacuum oscillation probabilities for the leading oscillation ( $1.267|\Delta m_{21}^2|L/E_\nu \ll 1$ ), appropriate for long-baseline experiments, are [46]

$$P(\nu_e \rightarrow \nu_\mu) = \sin^2 \theta_{23} \sin^2 2\theta_{13} \sin^2(1.267\Delta m_{32}^2 L/E_\nu), \quad (25)$$

$$P(\nu_e \rightarrow \nu_\tau) = \cos^2 \theta_{23} \sin^2 2\theta_{13} \sin^2(1.267\Delta m_{32}^2 L/E_\nu), \quad (26)$$

$$P(\nu_\mu \rightarrow \nu_\tau) = \cos^4 \theta_{13} \sin^2 2\theta_{23} \sin^2(1.267\Delta m_{32}^2 L/E_\nu). \quad (27)$$

These expressions are analogous to two-flavor vacuum oscillation probability in Eq. 21, except that each oscillation channel has a distinct amplitude that depends on the neutrino mixing parameters.

#### D. Matter effects

Electron neutrinos can elastically forward scatter off the electrons in matter via the charged current interaction [24]. When  $\nu_e$  oscillates into either  $\nu_\mu$  or  $\nu_\tau$ , this introduces an additional term in the diagonal element of the neutrino flavor evolution matrix corresponding to  $\nu_e \rightarrow \nu_e$ . It is useful to define the characteristic matter oscillation length  $L_0$  as the distance over which the phase of the  $\nu_e$  wavefunction changes by  $2\pi$  [25]:

$$L_0 = \frac{2\pi}{\sqrt{2}G_F N_e} \approx \frac{1.63 \times 10^4}{\rho(\text{g cm}^{-3}) Z/A} \text{ km}, \quad (28)$$

where  $N_e = \rho N_0 Z/A$  is the electron density in matter of density  $\rho$ ,  $Z/A$  is the average charge to mass ratio for the electrically neutral matter, and  $N_0$  is Avogadro's number. Note that, unlike the vacuum oscillation length  $L_V$ , the characteristic matter oscillation length  $L_0$  is independent of  $E_\nu$ . For ordinary rock ( $\rho \sim 3 \text{ g cm}^{-3}$  and  $Z/A = 0.5$ )  $L_0 \approx 10^4 \text{ km}$ . Matter effects are negligible when  $L_0 \gg L$  or  $L_0 \gg L_V$ . However, matter effects can be appreciable for trans-Earth experiments, where  $L \sim L_0$ , provided  $L_0 \lesssim L_V$  which is satisfied if  $\Delta m^2 (\text{eV}^2/c^4) \lesssim E(\text{GeV})/3000$ . In practice, for a trans-Earth experiment, if  $E_\mu$  is greater than a few tens of GeV the muon storage ring becomes too large to have it tilted at a large angle while preserving relatively long straight sections between the arcs. Hence, matter effects will only be important for a trans-Earth experiment if  $\Delta m^2 \leq O(10^{-2}) \text{ eV}^2/c^4$ . The tilt angle, distance, and average electron density for some representative long-baseline experiments from the Fermilab site are given in Table IV. For distances longer than about 10000 km the path goes through part of the core (the core diameter is 6960 km and the Earth's diameter is 12742 km).

The effective  $\nu_e$  oscillation length in matter  $L_m$  depends on  $L_0$  and  $L_V$ . Defining the ratio  $R_m \equiv L_m/L_V$ , it can be shown that [25,47]:

$$R_m \equiv \frac{L_m}{L_V} = \left[ 1 + \left( \frac{L_V}{L_0} \right)^2 - \frac{2L_V}{L_0} \cos 2\theta \right]^{-1/2}, \quad (29)$$

and

$$P(\nu_e \rightarrow \nu_x) = R_m^2 \sin^2(2\theta) \sin^2 \left[ \frac{1.267 \Delta m_{ji}^2 L}{R_m E_\nu} \right]. \quad (30)$$

For antineutrinos,  $N_e$  in Eq. 28 changes sign; hence matter effects are different for neutrinos and antineutrinos if  $\cos 2\theta \neq 0$ . If  $\cos 2\theta \Delta m_{ji}^2 > 0$  (i.e.,  $\nu_e$  is more closely associated with  $\nu_i$  than  $\nu_j$ ), oscillations of  $\nu_e$  are enhanced and oscillations of  $\bar{\nu}_e$  are suppressed when  $L_V \sim L_0$ ; if  $\cos 2\theta \Delta m_{ji}^2 < 0$ , the situation is reversed. Therefore, matter effects may distinguish between the two different mass orderings when  $\cos 2\theta \neq 0$ .

If  $L_V/L_0 = \cos 2\theta$ , the oscillations in matter have maximal mixing [25]. Figure 8 shows the values of  $\Delta m^2/E_\nu$  versus  $\sin^2 2\theta$  that give maximal mixing in the mantle and core of the Earth; similarly, Fig. 9 shows values of  $E_\nu$  versus  $\sin^2 2\theta$

that give maximal mixing in the Earth for  $\Delta m^2 = 3.5 \times 10^{-3} \text{ eV}^2/c^4$ , the value favored by the Super-Kamiokande atmospheric 708-day data [48].

Note that both the oscillation amplitude and the oscillation length depend on  $R_m$ , and hence on the density  $\rho$ . Fortunately, outside of the core the density profile of the Earth is well known, and is described by the Preliminary Reference Earth Model [49]. Density profiles along a selection of chords passing through the Earth are shown in Fig. 10. For  $L = 732 \text{ km}$  most of the pathlength is in rock with  $\rho \sim 2.5 \text{ g cm}^{-3}$ . For  $L = 7332 \text{ km}$  most of the pathlength is in higher density matter with  $\rho > 4 \text{ g cm}^{-3}$ . In some early studies [25,50] matter effects were computed using the average density  $\rho_{av}$  along the traversed path. This gives a reasonable estimate in many cases, but can introduce significant errors in the calculation of  $P(\nu_e \rightarrow \nu_x)$  in some regions of parameter space. To illustrate this, Fig. 11 shows  $P(\nu_e \rightarrow \nu_x)$ , for  $x = \mu$  or  $\tau$ , versus  $\rho$  calculated using Eq. 30 for 10 GeV neutrinos propagating 7332 km. The calculation assumes  $\sin^2 2\theta = 1$ , and the results are shown for three different values of  $\Delta m^2$ . For  $L = 7332 \text{ km}$  the average density is  $\rho_{av} = 4.2 \text{ g/cm}^3$ . Consider the  $\Delta m^2 = 0.001 \text{ eV}^2/c^4$  curve, for which  $L_V = 24800 \text{ km}$ . If  $\rho_{av}$  is used we obtain  $L_0 = 7810 \text{ km}$  and  $R_m = 0.30$ . The resulting oscillation probability is  $P(\rho_{av}) = 0.002$ . However, nearly all of the pathlength is through matter with densities that correspond to oscillation probabilities significantly higher than  $P(\rho_{av})$ . If the true density profile is used instead of  $\rho_{av}$  we obtain  $P = 0.014$ . Thus, in this example, using  $\rho_{av}$  leads to a result which underestimates the oscillation probability by a factor of 7. Therefore, in the following sections we do not use  $\rho_{av}$  to calculate  $P(\nu_e \rightarrow \nu_x)$ , but integrate using the density profile given by the preliminary Earth model. Extensive analyses have been made of oscillation effects involving transmission through the Earth's mantle and core [27,51–54].

For  $\nu_\mu$  oscillations to  $\nu_\tau$ , there are no matter effects for simple two-flavor oscillations (although there may be small matter effects on  $\nu_\mu \rightarrow \nu_\tau$  for three flavors [55]). For  $\nu_\mu \rightarrow \nu_s$  oscillations, however, muon neutrinos elastically forward scatter off the quarks and electrons in matter via the neutral current interaction, whereas sterile neutrinos do not. The matter oscillation length in this case can be found by replacing  $N_e$  in Eq. 28 by  $-N_n/2$  (by  $N_n/2$  for  $\bar{\nu}_\mu \rightarrow \bar{\nu}_s$  oscillations) [56];  $Z$  in Eq. 28 is then replaced by  $Z - A$  ( $A - Z$ ). If the mixing of atmospheric  $\nu_\mu$  is nearly maximal (as suggested by atmospheric neutrino data), then Eqs. 29 and 30 imply that the amplitude of  $\nu_\mu \rightarrow \nu_s$  and  $\bar{\nu}_\mu \rightarrow \bar{\nu}_s$  oscillations will both be suppressed by matter effects if  $L_V \gtrsim L_0$ , and by the same amount since  $\cos 2\theta \simeq 0$ .

### III. $\nu_\mu \rightarrow \nu_\tau$ AND $\nu_\mu \rightarrow \nu_s$ OSCILLATIONS

The currently favored explanation for the Super-Kamiokande atmospheric neutrino results is that muon neutrinos are oscillating primarily into either tau neutrinos or sterile neutrinos, with the oscillation parameters given by  $\sin^2 2\theta \sim 1$  and  $\Delta m^2$  in the approximate range  $0.002 \text{ eV}^2/c^4$  to  $0.006 \text{ eV}^2/c^4$  [4,48]. Searches for neutrino oscillations at accelerators are based on either the disappearance of the initial neutrino flavor, or the appearance of a neutrino flavor not originally within the neutrino beam. If the current interpretation of the Super-Kamiokande data is correct, the next generation of approved long baseline accelerator experiments [13,14] should confirm the existence of neutrino oscillations and make the first laboratory measurements of the oscillation parameters. This will happen in the period before a first muon storage ring neutrino source could be built. It is likely therefore that the main atmospheric neutrino oscillation physics goals in the muon storage ring neutrino source era would be to make very precise measurements of the oscillation parameters, and determine whether there is a small  $\nu_\mu \rightarrow \nu_s$  ( $\nu_\mu \rightarrow \nu_\tau$ ) component in a dominantly  $\nu_\mu \rightarrow \nu_\tau$  ( $\nu_\mu \rightarrow \nu_s$ ) signal. CC measurements can distinguish between  $\nu_\mu \rightarrow \nu_\tau$  and  $\nu_\mu \rightarrow \nu_s$  oscillations in two ways: (i) direct appearance of taus for  $\nu_\mu \rightarrow \nu_\tau$  [57] and (ii) a different  $\nu_\mu \rightarrow \nu_s$  transition probability due to matter effects when compared to  $\nu_\mu \rightarrow \nu_\tau$ . NC/CC measurements of  $\pi^0$  production can also distinguish  $\nu_\mu \rightarrow \nu_s$  from  $\nu_\mu \rightarrow \nu_\tau$  [58].

#### A. Fermilab $\rightarrow$ Gran Sasso

Consider first a 10 GeV muon storage ring at Fermilab with the neutrino beam-forming straight section pointing at Gran Sasso ( $L = 7332 \text{ km}$ ). The predicted CC event rates are listed as a function of  $E_\mu$  and  $\Delta m^2$  in Table V. The predicted  $\nu_\tau$  appearance event rates arising from  $\nu_\mu \rightarrow \nu_\tau$  oscillations with  $\sin^2 2\theta = 1$  and  $\Delta m^2$  in the range from  $0.002 \text{ eV}^2/c^4$  to  $0.006 \text{ eV}^2/c^4$  are only of order 1 event per kt-yr. This event rate is too low to enable a precise  $\nu_\tau$  appearance measurement in, for example, a 1 kt hybrid emulsion detector. However, an oscillation measurement could be made by a  $\nu_\mu$  disappearance experiment. In the absence of oscillations about 220  $\nu_\mu$  CC events would be expected per year in a 10 kt detector, with an event energy distribution peaking at  $\sim 10 \text{ GeV}$ . In the presence of oscillations the predicted  $\nu_\mu$  CC event rate (Table V) and the corresponding event energy distribution (Fig. 12) are both sensitive to  $\Delta m^2$  (provided  $\eta \sim 1$ ). However in general, for a given  $\Delta m^2$ , the average oscillation probability will depend on whether  $\nu_\mu \rightarrow \nu_\tau$  or  $\nu_\mu \rightarrow \nu_s$  or a mixture of the two oscillations is being observed. Hence, to avoid a large uncertainty

in the extracted value of  $\Delta m^2$  due to an uncertainty in which oscillation mode is being observed, it is desirable that a trans-Earth baseline experiment is sensitive to both  $\nu_\mu$  disappearance and  $\nu_\tau$  appearance. We conclude that the muon storage ring beam energy needs to be higher than 10 GeV to facilitate a  $\nu_\tau$  appearance measurement. Consider next a 20 GeV muon storage ring at Fermilab with the neutrino beam-forming straight section pointing at Gran Sasso ( $L = 7332$  km). The  $\nu_\tau$  CC rate corresponding to the favored region of  $\nu_\mu \rightarrow \nu_\tau$  parameter space is now sufficiently large to facilitate a  $\nu_\tau$  appearance measurement. In the absence of oscillations about 1900  $\nu_\mu$  CC events would be expected per year in a 10 kt detector. In the presence of  $\nu_\mu \rightarrow \nu_\tau$  oscillations with  $\sin^2 2\theta = 1$  and  $\Delta m^2 = 0.002 \text{ eV}^2/c^4$  ( $0.006 \text{ eV}^2/c^4$ ) only 370 (1300)  $\nu_\mu$  CC events per 10 kt-yr would be expected, together with 43 (14)  $\nu_\tau$  CC events per year in a 1 kt detector. The corresponding event rates for  $\nu_\mu \rightarrow \nu_s$  oscillations are 1400 (1200)  $\nu_\mu$  CC events per 10 kt-yr and no  $\nu_\tau$  CC events. With these trans-Earth event rates at a 20 GeV storage ring a  $\nu_\mu$  disappearance measurement would enable the oscillation probability to be measured with a precision of a few percent and, for a known mixture of  $\nu_\mu \rightarrow \nu_\tau$  and  $\nu_\mu \rightarrow \nu_s$  oscillations, would enable  $\Delta m^2$  to be determined with a statistical precision of a few percent. In addition, a  $\nu_\tau$  appearance measurement would enable the  $\nu_\mu \rightarrow \nu_\tau$  oscillation probability to be measured with a statistical precision which depends on  $\Delta m^2$ , but is typically about 20%. Finally, a comparison of the appearance and disappearance results would enable a  $\nu_\mu \rightarrow \nu_s$  contribution at the few times 10% level to be observed in a predominantly  $\nu_\mu \rightarrow \nu_\tau$  signal, or an approximately 10%  $\nu_\mu \rightarrow \nu_\tau$  contribution to be measured in a predominantly  $\nu_\mu \rightarrow \nu_s$  signal.

### B. Fermilab $\rightarrow$ Soudan

Consider a 10 GeV muon storage ring at Fermilab with the neutrino beam-forming straight section pointing at Soudan ( $L = 732$  km). Predicted event rates are listed in Table V. In the absence of oscillations about 22200  $\nu_\mu$  CC events would be expected per year in a 10 kt detector. In the presence of either  $\nu_\mu \rightarrow \nu_\tau$  or  $\nu_\mu \rightarrow \nu_s$  oscillations with  $\sin^2 2\theta = 1$  and  $\Delta m^2 = 0.002 \text{ eV}^2/c^4$  ( $0.006 \text{ eV}^2/c^4$ ) only 20500 (11700)  $\nu_\mu$  CC events per 10 kt-yr would be expected. In addition, for  $\nu_\mu \rightarrow \nu_\tau$  oscillations 20 (150)  $\nu_\tau$  CC events per year would be expected in a 1 kt detector. Note that the shape of the  $\nu_\tau$  CC interaction energy distribution (Fig. 13) exhibits some dependence on  $\Delta m^2$ , although a detector with good energy resolution would be needed to exploit this dependence. We conclude that a storage ring with a beam energy as low as 10 GeV might be of interest for a Fermilab  $\rightarrow$  Soudan experiment, particularly if  $\Delta m^2$  is at the upper end of the currently favored region. In this case the average oscillation probability could be measured with a statistical precision of better than 1% from the disappearance measurement, and the resulting  $\Delta m^2$  be determined with a precision of  $\sim 1\%$ . Note that, since matter effects are small, there is no additional uncertainty on  $\Delta m^2$  arising from an imprecise knowledge of the oscillation mode ( $\nu_\mu \rightarrow \nu_\tau$  or  $\nu_\mu \rightarrow \nu_s$ ). Finally, with  $\Delta m^2 = 0.006 \text{ eV}^2/c^4$ , a comparison of the  $\nu_\mu$  disappearance and  $\nu_\tau$  appearance measurements would enable a few percent contribution from  $\nu_\mu \rightarrow \nu_\tau$  oscillations to be measured in a predominantly  $\nu_\mu \rightarrow \nu_s$  signal, or a few times 10%  $\nu_\mu \rightarrow \nu_s$  contribution to be measured in a predominantly  $\nu_\mu \rightarrow \nu_\tau$  signal.

In Fig. 14 single  $\nu_\tau$  CC event per kt-yr contours in the  $(\sin^2 2\theta, \Delta m^2)$ -plane are shown for  $L = 732$  km as a function of  $E_\mu$ . The sensitivity of the  $\nu_\tau$  appearance measurement increases with increasing muon storage ring beam energy. Consider the sensitivity for a 50 GeV muon storage ring. The dependence of the  $\nu_\tau$  CC rates on  $\sin^2 2\theta$  and  $\Delta m^2$  is shown in Fig. 15. The predicted event rates range from several hundred events per kt-yr at the lower end of the Super-Kamiokande allowed region of parameter space, to several thousand events per kt-yr at the upper end of the favored region (Table V). Hence the  $\nu_\mu \rightarrow \nu_\tau$  oscillation probability could be measured with a precision of a few percent, corresponding to a determination of  $\Delta m^2$  with a precision of a few percent. However, the predicted oscillation probabilities are small, and the statistical precision of the disappearance measurement is less than the corresponding precision for the  $E_\mu = 10$  GeV case. Note that about 2 million  $\nu_\mu$  CC events would be expected per year in a 10 kt detector. The sensitivity of the disappearance measurement may therefore be limited by systematics. This needs further study. We conclude that, although the statistical sensitivity of the  $\nu_\tau$  appearance measurement improves with increasing  $E_\mu$ , the optimum choice of muon beam energy depends upon whether  $\Delta m^2$  is in the lower or upper part of the favored region of parameter space, and on at what level the higher energy experiments would be limited by systematics.

### C. $L = 7332$ km versus 732 km

The relative performance of experiments at long ( $L = 732$  km) and very long ( $L = 7332$  km) baselines depends on both  $\Delta m^2$  and the oscillation mode ( $\nu_\mu \rightarrow \nu_\tau$  or  $\nu_\mu \rightarrow \nu_s$ ). Based on the results summarized in Table V we find that:



Case 1:  $0.002 < \Delta m^2 < 0.004 \text{ eV}^2/\text{c}^4$  and  $\nu_\mu \rightarrow \nu_\tau$  oscillations dominate. An  $L = 732 \text{ km}$  experiment with  $E_\mu = 10\text{-}20 \text{ GeV}$ , or an  $L = 7332 \text{ km}$  experiment with  $E_\mu = 20 \text{ GeV}$  both seem interesting. A higher energy  $L = 732 \text{ km}$  experiment (e.g.  $E_\mu = 50 \text{ GeV}$ ) would provide a higher statistics measurement of the  $\nu_\mu \rightarrow \nu_\tau$  oscillation probability, but the oscillation probability is small and the measurement precision may be dominated by systematics.

Case 2:  $0.004 < \Delta m^2 < 0.006 \text{ eV}^2/\text{c}^4$  and  $\nu_\mu \rightarrow \nu_\tau$  oscillations dominate. An  $L = 732 \text{ km}$  experiment with  $E_\mu = 10\text{-}20 \text{ GeV}$  would provide a good  $\nu_\mu$  disappearance measurement and a good  $\nu_\tau$  appearance measurement. With a larger  $E_\mu$  (e.g.  $50 \text{ GeV}$ ) the unoscillated neutrino CC rate becomes large and the oscillation measurements may be limited by systematics. The trans-Earth baseline option with  $E_\mu = 20 \text{ GeV}$  yields less statistical precision than the  $L = 732 \text{ km}$  option with  $E_\mu = 20 \text{ GeV}$ .

Case 3:  $\nu_\mu \rightarrow \nu_s$  oscillations dominate. In this case a very sensitive  $\nu_\mu$  disappearance measurement is important. A low energy ( $10 \text{ GeV}$ ) storage ring pointing at Soudan seems attractive, particularly if  $\Delta m^2$  is in the upper half of the favored region. An  $L = 7332 \text{ km}$  baseline experiment seems to be less attractive than an  $L = 732 \text{ km}$  baseline experiment for large  $\Delta m^2$ , but is complementary to the shorter baseline experiment for small  $\Delta m^2$ , and would enable matter effects to be measured.

#### IV. $\nu_e \rightarrow \nu_\mu$ OSCILLATIONS

If confirmed, the LSND neutrino oscillation results necessarily imply the existence of  $\nu_e \rightarrow \nu_\mu$  oscillations, with  $0.3 < \Delta m_{LSND}^2 < 2.0 \text{ eV}^2/\text{c}^4$ . Oscillation limits from the Karmen experiment [59] are no longer in conflict with the LSND effect. In addition, the solar neutrino results can also be interpreted in terms of  $\nu_e \rightarrow \nu_\mu$  and/or  $\nu_e \rightarrow \nu_\tau$  oscillations either within the framework of the MSW effect with  $\Delta m_{sun}^2 \sim 5 \times 10^{-5} \text{ eV}^2/\text{c}^4$  and  $\sin^2 2\theta \sim 0.8$  (large angle solution) or  $\Delta m_{sun}^2 \sim 5 \times 10^{-6} \text{ eV}^2/\text{c}^4$  and  $\sin^2 2\theta \sim 5 \times 10^{-3}$  (small angle solution) [60–62], or within the framework of vacuum oscillations [63] with  $\Delta m_{sun}^2 \sim 0.65\text{--}8.6 \times 10^{-10} \text{ eV}^2/\text{c}^4$  [8,60]. In the context of three neutrinos, although the primary oscillation of atmospheric neutrinos is  $\nu_\mu \rightarrow \nu_\tau$ , a small  $\nu_\mu \rightarrow \nu_e$  component is not excluded. For  $\Delta m_{atm}^2 \sim 3.5 \times 10^{-3} \text{ eV}^2/\text{c}^4$ , a measurement of  $\nu_e \rightarrow \nu_\mu$  will place strong limits on  $\sin^2 \theta_{23} \sin^2 2\theta_{13}$  (see Eq. 25) [6,8].

The next generation of approved neutrino experiments include MiniBooNE [64] at Fermilab, and KamLAND [17] at the Kamioka Mine, Japan. MiniBooNE, which will consist of a 445 ton fiducial volume liquid scintillator detector 500 m downstream of a  $\nu_\mu$  source, with  $E_\nu \sim 0.75 \text{ GeV}$ , should confirm or refute the neutrino oscillation interpretation of the LSND results. KamLAND, which will consist of a 1 kt liquid scintillator detector 140 km and 200 km from reactors in Japan, should observe a  $\nu_e$  disappearance signal if the solar neutrino results are due to oscillations corresponding to the large angle MSW solution. Both MiniBooNE and KamLAND nominally begin operation in  $\sim 2001$ . In the following we consider the  $\nu_e \rightarrow \nu_\mu$  physics potential of a muon storage ring neutrino source in the post-MiniBooNE/KamLAND era.

##### A. Fermilab $\rightarrow$ Soudan

Figure 16 shows single event per year contours in the  $(\sin^2 2\theta, \Delta m^2)$ -plane for  $\nu_\mu$  CC interactions in a 10 kt detector 732 km downstream of the muon storage ring neutrino source described in Section II.A, where the  $\nu_\mu$  arise from  $\nu_e \rightarrow \nu_\mu$  oscillations. The contours are shown for several values of  $E_\mu$  from 10 GeV up to 250 GeV. The upper part of the MSW large mixing angle solution is within the single-event per year boundary for  $E_\mu \geq 10 \text{ GeV}$ . The sensitivity improves with increasing  $E_\mu$ . The event rate is shown in the  $\sin^2 2\theta\text{--}\Delta m^2$  plane in Fig. 17 for  $E_\mu = 250 \text{ GeV}$ . To completely cover the parameter space corresponding to the MSW large mixing angle solution would require larger muon beam currents than those of the scenario described in Section II.A. It should be noted that the full muon collider front-end described in Ref. [32], would produce a factor of 3.3 more muons. The resulting neutrino flux would just about enable the entire MSW large mixing angle solution to be covered by a 50 GeV storage ring and a few years of running with, for example, a 20 kt detector having a detection efficiency of 50%, provided background rates are negligible. The small angle MSW solution is out of reach of a muon storage ring neutrino source, as currently envisioned. Hence if KamLAND rules out the large angle solution, then solar neutrino oscillations would provide little motivation for a Fermilab  $\rightarrow$  Soudan  $\nu_e \rightarrow \nu_\mu$  appearance experiment. On the other hand, should KamLAND obtain a positive signal for solar neutrino oscillations corresponding to the large angle MSW solution, a Fermilab  $\rightarrow$  Soudan muon storage ring neutrino source experiment to search for  $\nu_e \rightarrow \nu_\mu$  appearance might be feasible, but would clearly be challenging and would probably require the full muon collider muon source for several years. If this becomes the only way to

discover whether the solar neutrino oscillations are due to  $\nu_e \rightarrow \nu_\mu$  or due to  $\nu_e \rightarrow \nu_\tau$  or  $\nu_s$ , then this experiment would certainly be worthy of serious consideration.

Independent of the KamLAND results, a positive MiniBooNE result would motivate precise measurements of  $\nu_e \rightarrow \nu_\mu$  oscillations to test whether or not  $P(\nu_e \rightarrow \nu_\mu) = P(\nu_\mu \rightarrow \nu_e)$  ( $T$  invariance), test the oscillation phenomenon with a very different  $L$  and  $E_\nu$ , search for a  $\nu_e \rightarrow \nu_s$  contribution, etc. A Fermilab  $\rightarrow$  Soudan  $\nu_e \rightarrow \nu_\mu$  experiment would enable many thousands of  $\nu_\mu$  appearance CC interactions (due to LSND-scale oscillations) to be measured (see Figs. 16 and 17). Such measurements could also test the existence of  $\nu_e \rightarrow \nu_\mu$  oscillations at the atmospheric  $\Delta m^2$  scale ( $\sim 3.5 \times 10^{-3} \text{ eV}^2/\text{c}^4$ ), which allows a precise determination of the three-neutrino mixing parameter  $\cos^2 \theta_{23} \sin^2 2\theta_{13}$ .

## B. Matter effects

Figure 18 shows single event per year contours in the  $(\sin^2 2\theta, \Delta m^2)$ -plane for  $\nu_\mu$  CC interactions in a 10 kt detector 7332 km downstream of the muon storage ring neutrino source described in Section II.A, where the  $\nu_\mu$  arise from  $\nu_e \rightarrow \nu_\mu$  oscillations with  $\Delta m^2 > 0$ . The contours are shown for  $E_\mu = 10, 20, 50,$  and  $250$  GeV. Figure 19 shows the corresponding contours for  $\bar{\nu}_e \rightarrow \bar{\nu}_\mu$  oscillations. Compared with the equivalent contours for  $L = 732$  km (Fig. 16) the lower event statistics suppress the sensitivity at large  $\Delta m^2$  and small  $\sin^2 2\theta$ , and matter effects (Eq. 30) suppress the sensitivity at small  $\Delta m^2$  and large  $\sin^2 2\theta$ . It is interesting to consider whether the matter effects might be measured by a trans-Earth muon storage ring neutrino source  $\nu_e \rightarrow \nu_\mu$  experiment searching for wrong-sign muons.

Note that if MiniBooNE confirms the LSND evidence for oscillations, then  $\Delta m^2$  will be too large to result in a significant modification of the oscillation probability due to matter effects. However, if KamLAND obtains a positive  $\nu_e$  disappearance result corresponding to the large mixing angle MSW solution for solar neutrino oscillations, then the  $\Delta m^2$  will be in the right range to produce a significant modification of the oscillation probability due to matter. As an example, consider a storage ring with  $E_\mu = 20$  GeV, and assume that  $\sin^2 2\theta = 1$ . Then if  $\Delta m^2 = 1 \times 10^{-4} \text{ eV}^2/\text{c}^4$ , in the absence of matter effects  $\sim 11$  wrong sign muons (from  $\nu_e \rightarrow \nu_\mu$  oscillations) would be expected per 10 kt-yr. With matter effects, the number of wrong sign muons is reduced to  $\sim 0.6$  per 10 kt-yr. Hence, an experiment to measure matter effects, by comparing the wrong sign muon rates in a long baseline (e.g  $L = 732$  km) experiment with the corresponding rates in a trans-Earth (e.g  $L = 7332$  km) experiment might be feasible if the solar neutrino results are due to  $\nu_e \rightarrow \nu_\mu$  oscillations with  $\sin^2 2\theta \sim 1$  and  $\Delta m^2$  at the upper end of the region of allowed parameter space for the MSW large mixing angle solution. This experiment would clearly be challenging, and would probably need a more intense neutrino source than described in Section II.A (for example, the full muon collider muon source utilized for several years with a 20 kt detector).

If there is a small  $\nu_\mu \rightarrow \nu_e$  and  $\bar{\nu}_\mu \rightarrow \bar{\nu}_e$  component to atmospheric neutrino oscillations, then  $\nu_e \rightarrow \nu_\mu$  and  $\bar{\nu}_e \rightarrow \bar{\nu}_\mu$  oscillations are also expected; a trans-Earth experiment could test for different matter effects acting on these two oscillation channels. Table VI shows, for a Fermilab  $\rightarrow$  Gran Sasso experiment ( $L = 7332$  km), the  $\nu_e \rightarrow \nu_\mu$  and  $\bar{\nu}_e \rightarrow \bar{\nu}_\mu$  oscillation probabilities, the predicted numbers of  $\nu_\mu$  and  $\bar{\nu}_\mu$  CC appearance events, and the average probability for  $\nu_e \rightarrow \nu_\mu$  assuming no matter effects. The predictions are tabulated for  $\sin^2 2\theta = 0.1$  with various  $E_\mu$  and values of  $\Delta m^2 > 0$  suggested by the atmospheric neutrino data. If  $\Delta m^2 < 0$  (i.e., the lower mass eigenstate is more closely associated with  $\nu_\mu$  and not  $\nu_e$ ), then the oscillation probabilities for neutrinos and antineutrinos in Table VI are reversed. Thus the sign of  $\Delta m^2$  may be determined from these measurements if matter effects are present [25,27].

In this paper we have assumed that the neutrino mixing conserves  $CP$ ; the apparent violation of  $CP$  in the  $\nu_e \rightarrow \nu_\mu$  and  $\bar{\nu}_e \rightarrow \bar{\nu}_\mu$  channels would be due to matter effects. Measuring  $\nu_\mu \rightarrow \nu_e$  and  $\bar{\nu}_\mu \rightarrow \bar{\nu}_e$  oscillations as well (through an electron appearance experiment) would provide important cross-checks and help distinguish between matter effects and  $CP$  violation. For example,  $CPT$  conservation for vacuum oscillations implies  $P(\nu_e \rightarrow \nu_\mu) = P(\bar{\nu}_\mu \rightarrow \bar{\nu}_e)$ , whether  $CP$  is violated or not, so that a difference between these two oscillation probabilities would be unambiguous evidence for matter effects. Similarly, matter effects are the same for  $\nu_e \rightarrow \nu_\mu$  and  $\nu_\mu \rightarrow \nu_e$  oscillations, so that a difference between these oscillation channels is due to  $T$  violation, which in turn implies  $CP$  violation under the plausible assumption that  $CPT$  is conserved.

## V. $\nu_e \rightarrow \nu_\tau$ OSCILLATIONS

If the atmospheric neutrino results are due to  $\nu_\mu \rightarrow \nu_\tau$  oscillations with a  $\Delta m^2 \sim 3.5 \times 10^{-3} \text{ eV}^2/\text{c}^4$ , and the solar neutrino results are due to  $\nu_e \rightarrow \nu_\mu$  and/or  $\nu_e \rightarrow \nu_\tau$  oscillations with a  $\Delta m^2 \leq \text{O}(10^{-5}) \text{ eV}^2/\text{c}^4$ , it is tempting to conclude that  $\nu_e \rightarrow \nu_\tau$  oscillations should exist with an associated  $\Delta m^2 = \text{O}(10^{-3}) \text{ eV}^2/\text{c}^4$ , but with unknown effective  $\sin^2 2\theta$ . For  $\Delta m^2 > 2 \times 10^{-3} \text{ eV}^2/\text{c}^4$ ,  $\nu_e \rightarrow \nu_\tau$  oscillations with  $\sin^2 2\theta > 0.2$  are already excluded by the CHOOZ

reactor  $\nu_e$  disappearance experiment, although there is no limit for  $\Delta m^2 < 10^{-3} \text{ eV}^2/c^4$ . In a three-neutrino scenario, measurements of atmospheric neutrinos indicate  $\sin^2 2\theta_{23} > 0.8$  and exclude  $\sin^2 2\theta_{13} > 0.33$  for all atmospheric  $\Delta m^2$  [7];  $\nu_e \rightarrow \nu_\tau$  oscillations may be detectable if  $\theta_{13}$  is not too small. Hence, the region of parameter space that would be interesting to cover in future  $\nu_e \rightarrow \nu_\tau$  oscillation searches is given by  $\Delta m^2 \sim 3.5 \times 10^{-3} \text{ eV}^2/c^4$  and effective  $\sin^2 2\theta < 0.3$ .

Consider first a  $\nu_e \rightarrow \nu_\tau$  appearance experiment. Event rates are summarized in Table VII for the neutrino source described in Section II.A, and  $\sin^2 2\theta = 0.1$ . For a baseline length of 732 km matter effects are small, and hence the oscillation rates for  $\sin^2 2\theta < 0.1$  can be obtained by multiplying the rates in the table with the value of  $\sin^2 2\theta/0.1$ . For a baseline length of 7332 km matter effects are large and enhance the  $\nu_\tau$  appearance rate for  $\Delta m^2 \sim 5 \times 10^{-3} \text{ eV}^2/c^4$ , although the numbers of events are not large. On the other hand, the corresponding rates for a 1 kt detector 732 km downstream yield more  $\nu_\tau$  appearance events in the region of interest, and for  $E_\mu = 50 \text{ GeV}$  could yield up to a few events per year with  $\sin^2 2\theta$  as small as  $10^{-2}$  (see Fig. 20). Single-event per kt-yr sensitivity contours in the  $(\sin^2 2\theta, \Delta m^2)$ -plane are shown versus the stored muon energy in Fig. 21. Decreasing the storage ring energy from 50 GeV to 20 GeV would increase the minimum  $\sin^2 2\theta$  that could be probed by a factor of a few.

In a three-neutrino scenario, a 1 kt detector 732 km downstream could probe  $\cos^2 \theta_{23} \sin^2 2\theta_{13}$  to very low values; when combined with  $\nu_e \rightarrow \nu_\mu$  measurements (see Sec. IV) and with future atmospheric neutrino results, a precise determination of  $\theta_{23}$ ,  $\theta_{13}$  and  $\Delta m^2$  should be possible.

## VI. SUMMARY

In this paper we have made a comprehensive study of possible neutrino oscillation measurements in long-baseline experiments with an intense neutrino beam from a muon storage ring. Our results can be summarized as follows:

- (i) A neutrino beam from a muon storage ring provides much larger electron neutrino interaction rates than conventional neutrino beams, and much larger muon neutrino interaction rates if  $E_\mu \geq 20 \text{ GeV}$ .
- (ii) If the  $\Delta m^2$  associated with the atmospheric neutrino results is in the lower part of the allowed Super-Kamiokande parameter space ( $\Delta m^2 < 4 \times 10^{-3} \text{ eV}^2/c^4$ ), a Fermilab  $\rightarrow$  Gran Sasso trans-Earth experiment with an  $E_\mu = 20 \text{ GeV}$  muon storage ring neutrino source would enable  $\nu_\mu$  disappearance to be established in an accelerator-based experiment, and  $\Delta m^2$  to be measured with a precision of a few percent. Matter effects may also allow the differentiation of  $\nu_\mu \rightarrow \nu_\tau$  and  $\nu_\mu \rightarrow \nu_s$  oscillations.
- (iii) If the  $\Delta m^2$  associated with the atmospheric neutrino results is in the upper part of the allowed Super-Kamiokande/Kamiokande parameter space ( $\Delta m^2 > 4 \times 10^{-3} \text{ eV}^2/c^4$ ), a Fermilab  $\rightarrow$  Soudan (or CERN  $\rightarrow$  Gran Sasso)  $\nu_\mu$  disappearance experiment would allow  $\Delta m^2$  to be measured with a precision of a few percent; a  $\nu_\tau$  appearance experiment would enable a search for a small contribution from  $\nu_\mu \rightarrow \nu_s$  within a dominantly  $\nu_\mu \rightarrow \nu_\tau$  signal, or conversely, a small contribution from  $\nu_\mu \rightarrow \nu_\tau$  within a dominantly  $\nu_\mu \rightarrow \nu_s$  signal.
- (iv) If the LSND  $\nu_\mu \rightarrow \nu_e$  oscillation results are confirmed by MiniBooNE, a Fermilab  $\rightarrow$  Soudan  $\nu_e \rightarrow \nu_\mu$  experiment would enable many thousands of wrong-sign muons to be measured, facilitate a precise confirmation and measurement of the oscillation parameters, and enable  $P(\nu_\mu \rightarrow \nu_e)$  to be compared with  $P(\nu_e \rightarrow \nu_\mu)$  for a test of  $T$  invariance.
- (v) If KamLAND observes  $\nu_e$  disappearance with a rate corresponding to the large angle MSW solar neutrino solution then a measurement of  $\nu_e \rightarrow \nu_\mu$  appearance might be conceivable for a Fermilab  $\rightarrow$  Soudan experiment if the full muon source needed for a muon collider were available for several years of running with a muon storage ring neutrino source. It might also be possible to measure matter effects as the electron neutrinos traverse the Earth. These measurements are however challenging and need further consideration to assess their viability.
- (vi) If there is a small but non-negligible component of  $\nu_\mu \leftrightarrow \nu_e$  oscillations in atmospheric neutrinos, a Fermilab  $\rightarrow$  Gran Sasso measurement of  $\nu_e \rightarrow \nu_\mu$  and  $\bar{\nu}_e \rightarrow \bar{\nu}_\mu$  could perhaps detect matter effects in the oscillation, which show up as apparent  $CP$  violation. Matter effects and true  $CP$  violation can be distinguished by also measuring  $\nu_\mu \rightarrow \nu_e$  and  $\bar{\nu}_\mu \rightarrow \bar{\nu}_e$  oscillations: a nonzero  $P(\nu_e \rightarrow \nu_\mu) - P(\nu_\mu \rightarrow \nu_e)$  signals  $T$  (and hence  $CP$ ) violation, a nonzero  $P(\nu_e \rightarrow \nu_\mu) - P(\bar{\nu}_\mu \rightarrow \bar{\nu}_e)$  signals matter effects, while a nonzero  $P(\nu_e \rightarrow \nu_\mu) - P(\bar{\nu}_e \rightarrow \bar{\nu}_\mu)$  can occur due to either matter or  $CP$  violation. If oscillations of neutrinos are enhanced and antineutrinos suppressed, then  $\Delta m^2 > 0$ ; for the reverse situation,  $\Delta m^2 < 0$ .

- (vii) A  $\nu_e \rightarrow \nu_\tau$  appearance search sensitive to  $\Delta m^2 \text{ O}(10^{-3}) \text{ eV}^2/c^4$  and  $\sin^2 2\theta$  down to about  $10^{-2}$  seems possible with a Fermilab  $\rightarrow$  Soudan experiment using a  $\geq 20$  GeV muon storage ring. Higher energies are more desirable for  $\nu_\tau$  appearance experiments.
- (viii) In a three-neutrino scenario with different  $\Delta m^2$  scales for the solar and atmospheric oscillations, measurements of  $\nu_e \rightarrow \nu_\mu$  and  $\nu_e \rightarrow \nu_\tau$  should provide an accurate determination of the two mixing angles associated with the leading oscillation. When combined with solar neutrino measurements, the three-neutrino mixing parameters would be completely determined, except for a possible  $CP$  violating phase.

#### ACKNOWLEDGMENTS

The authors would like to thank D. Casper and J. Morphin for providing tables of neutrino cross sections, E. Kearns and J. Learned for useful correspondence, and J. Hlyen, S. Parke and T. Weiler and for discussions. Part of this work was performed at the Fermi National Accelerator Laboratory, which is operated by Universities Research Association, under contract DE-AC02-76CH03000 with the U.S. Department of Energy. This work was supported in part by the U.S. Department of Energy, Division of High Energy Physics, under Grants No. DE-FG02-94ER40817, and No. DE-FG02-95ER40896, and in part by the University of Wisconsin Research Committee with funds granted by the Wisconsin Alumni Research Foundation.

- 
- [1] See for example B. Kayser, “Neutrino mass: Where do we stand, and where are we going ?”, hep-ph/9810513, 28 Oct. 1998; J. Conrad, “Recent results on neutrino oscillations”, hep-ex/9811009, 5 Nov. 1998.
- [2] B.T. Cleveland *et al.*, Nucl. Phys. B (Proc. Suppl.) **38**, 47 (1995); GALLEX collaboration, W. Hampel *et al.*, Phys. Lett. **B388**, 384 (1996); SAGE collaboration, J.N. Abdurashitov *et al.*, Phys. Rev. Lett. **77**, 4708 (1996); Kamiokande collaboration, Y. Fukuda *et al.*, Phys. Rev. Lett. **77**, 1683 (1996); Super-Kamiokande collaboration, Y. Fukuda *et al.*, Phys. Rev. Lett. **82**, 2430 (1999); Phys. Rev. Lett. **82**, 1810 (1999).
- [3] See, e.g., J.N. Bahcall, S. Basu, and M.H. Pinsonneault, Phys. Lett. **B 433**, 1 (1998), and references therein.
- [4] Super-Kamiokande Collaboration, Y. Fukuda *et al.*, Phys. Lett. **B433**, 9 (1998); Phys. Lett. **B436**, 33 (1998); Phys. Rev. Lett. **81**, 1562 (1998); Phys. Rev. Lett. **82**, 2644 (1999).
- [5] Kamiokande collaboration, K.S. Hirata *et al.*, Phys. Lett. **B280**, 146 (1992); Y. Fukuda *et al.*, Phys. Lett. **B335**, 237 (1994); IMB collaboration, R. Becker-Szendy *et al.*, Nucl. Phys. Proc. Suppl. **38B**, 331 (1995); Soudan-2 collaboration, W.W.M. Allison *et al.*, Phys. Lett. **B391**, 491 (1997); MACRO collaboration, M. Ambrosio *et al.*, Phys. Lett. **B434**, 451 (1998).
- [6] G.L. Fogli, E. Lisi, A. Marrone, and G. Scioscia, Phys. Rev. **D59**, 033001 (1999).
- [7] V. Barger, T.J. Weiler, and K. Whisnant, Phys. Lett. **B440**, 1 (1998).
- [8] V. Barger and K. Whisnant, Phys. Rev. **D59**, 093007 (1999).
- [9] R. Barbieri, L.J. Hall, D. Smith, A. Strumia, and N. Weiner, JHEP 9812, 017 (1998).
- [10] C. Athanassopoulos *et al.* (LSND Collab.), Phys. Rev. Lett. **77**, 3082 (1996).
- [11] C. Athanassopoulos *et al.* (LSND Collab.), Phys. Rev. Lett. **81**, 1774 (1998).
- [12] S.M. Bilenky, C. Giunti, and W. Grimus, Eur. Phys. J. **C1**, 247 (1998); V. Barger, S. Pakvasa, T.J. Weiler, and K. Whisnant, Phys. Rev. **D58**, 093016 (1998).
- [13] K. Nishikawa *et al.* (KEK-PS E362 Collab.), “Proposal for a Long Baseline Neutrino Oscillation Experiment, using KEK-PS and Super-Kamiokande”, 1995, unpublished; INS-924, April 1992, submitted to J.Phys.Soc.Jap.; Y. Oyama, Proc. of the YITP Workshop on Flavor Physics, Kyoto, Japan, 1998, hep-ex/9803014.
- [14] MINOS Collaboration, “Neutrino Oscillation Physics at Fermilab: The NuMI-MINOS Project,” NuMI-L-375, May 1998.
- [15] CHOOZ Collaboration, M. Apollonio *et al.*, Phys. Lett. **B420**, 320 (1998).
- [16] Y. Declais *et al.*, Nucl. Phys. **B434**, 503 (1995).
- [17] P. Alivisatos *et al.*, “KamLAND Proposal”, Preprint Stanford-HEP-98-03; G. Gratta, hep-ex/9905011, “Neutrino oscillation experiments at nuclear reactors,” Proc. of the 17th International workshop on Weak Interactions and Neutrinos (WIN99), Cape Town, South Africa, Jan. 1999.
- [18] Palo Verde Collaboration, F. Boehm *et al.*, Prog. Art. Nucl. Phys. **40**, 253 (1998).
- [19] S. Geer, Phys. Rev. **D57**, 6989 (1998).
- [20] A. De Rujula, M.B. Gavela, and P. Hernandez, Nucl. Phys. **B547**, 21 (1999).
- [21] M. Campanelli, A. Bueno, and A. Rubbia, hep-ph/9905240.
- [22] P. Lipari and M. Lusignoli, Phys. Rev. **D58**, 073005 (1998); Q.Y. Liu and A. Yu. Smirnov, Nucl. Phys. **B524**, 505 (1998); R. Foot, R.R. Volkas, and O. Yasuda, Phys. Rev. **D58**, 013006 (1998); M.C. Gonzalez-Garcia, H. Nunokawa, O. Peres, and J.W.F. Valle, Nucl. Phys. **B543**, 2 (1999).
- [23] T. Blazek, S. Raby, and K. Tobe, hep-ph/9903340.
- [24] L. Wolfenstein, Phys. Rev. **D17**, 2369 (1978); S.P. Mikheyev and A. Smirnov, Yad. Fiz. **42**, 1441 (1985) [Sov. J. Nucl. Phys. **42**, 913 (1986)]; Nuovo Cim. **C 9**, 17 (1986).
- [25] V. Barger, K. Whisnant, S. Pakvasa, and R.J.N. Phillips, Phys. Rev. **D22**, 2718 (1980).
- [26] P. Langacker, J.P. Leveille, and J. Sheiman, Phys. Rev. **D 27**, 1228 (1983).
- [27] P. Lipari, hep-ph/9903481.
- [28] N. Cabbibo, Phys. Lett. **B72**, 333 (1978).
- [29] V. Barger, K. Whisnant, R.J.N. Phillips, Phys. Rev. Lett. **45**, 2084 (1980)
- [30] S. Pakvasa, in *Proc. of the XXth International Conference on High Energy Physics*, ed. by L. Durand and L.G. Pondrum, AIP Conf. Proc. No. 68 (AIP, New York, 1981), Vol. 2, pp.1164.
- [31] For recent discussions of  $CP$  violation effects in neutrino oscillations, see V. Barger, Y.-B. Dai, K. Whisnant, and B.-L. Young, Phys. Rev. **D59**, 113010 (1999); D.J. Wagner and T.J. Weiler, Phys. Rev. **D59**, 113007 (1999); A.M. Gago, V. Pleitez, R.Z. Funchal, hep-ph/9810505; K.R. Schubert, hep-ph/9902215; K. Dick, M. Freund, M. Lindner and A. Romanino, hep-ph/9903308; J. Bernabeu, hep-ph/9904474; S.M. Bilenky, C. Giunti, and W. Grimus, Phys. Rev. **D58**, 033001 (1998); M. Tanimoto, Prog. Theor. Phys. **97**, 901 (1997); J. Arafune, J. Sato, Phys. Rev. **D55**, 1653 (1997); T. Fukuyama, K. Matasuda, H. Nishiura, Phys. Rev. **D57**, 5844 (1998); M. Koike and J. Sato, hep-ph/9707203, Proc. of the KEK Meetings on CP Violation and its Origin; H. Minakata and H. Nunokawa, Phys. Lett. **B413**, 369 (1997); H. Minakata and H. Nunokawa, Phys. Rev. **D57**, 4403 (1998); J. Arafune, M. Koike and J. Sato, Phys. Rev. **D56**, 3093 (1997); M. Tanimoto,

- Phys. Lett. **B435**, 373 (1998).
- [32] “Status of Muon Collider Research and Development and Future Plans”, C. Ankenbrandt et al. (The Muon Collider Collaboration), Fermilab-Pub-98/179, Physics Review Special Topics: Accelerators and Beams, in press.
- [33] Workshop on the Potential for Neutrino Physics at Future Muon Colliders, Brookhaven National Laboratory, 13-14 August, 1998, see <http://pubweb.bnl.gov/people/bking/nushop/workshop.html>
- [34] “Muon Storage Rings at CERN”; <http://muonstoragerings.cern.ch/Welcome.html/>
- [35] V. Barger, T.J. Weiler, and K. Whisnant, Phys. Lett. **B427**, 97 (1998).
- [36] A. Bueno, M. Campanelli, and A. Rubbia, hep-ph/9808485; hep-ph/9809252; B. Autin et al., CERN-SPSC/98-30; M. Doucet, J. Panman, and P. Zucchelli, hep-ex/9905029; S. Dutta, R. Gandhi, and B. Mukhopadhyaya, hep-ph/9905475.
- [37] S. Geer, C. Johnstone, and D. Neuffer, “Muon Storage Ring Neutrino Source: The Path to a Muon Collider ?”, FERMILAB-TM-2073, 1999; “Design concepts for a muon storage ring neutrino source,” FERMILAB-PUB-99/121.
- [38] S. Holmes et al., “A Development Plan for the Fermilab Proton Source,” FERMILAB-TM-2021, September 1997, unpublished.
- [39] D. Finley, S. Geer, and J. Sims, “Muon Colliders: A vision for the future of Fermilab,” FERMILAB-TM-2072, 1999.
- [40] B. Autin, talk at Muon Collider Collaboration Workshop, St. Croix, May 1999.
- [41] See for example: T. K. Gaisser, “Cosmic Rays and Particle Physics,” Cambridge University Press 1990.
- [42] H.M. Gallagher and M. Goodman, “Neutrino Cross Sections”, NuMI-112, November 1995; J. Morphin, private communication.
- [43] D. Casper, private communication.
- [44] Z. Maki, M. Nakagawa, and S. Sakata, Prog. Theor. Phys. **28**, 870 (1962).
- [45] L. Wolfenstein, Phys. Lett. **B 107**, 77 (1981); P.B. Pal and L. Wolfenstein, Phys. Rev. **D 25**, 766 (1982); F. del Aguila and M. Zralek, Nucl. Phys. **B447**, 211 (1995); Acta Phys. Pol. **B27**, 971 (1996).
- [46] V. Barger, K. Whisnant, R.J.N. Phillips, Phys. Rev. **D22**, 1636 (1980).
- [47] T.K. Kuo and J. Pantaleone, Rev. Mod. Phys. **61**, 937 (1989).
- [48] Y. Totsuka, talk at *The Innerspace-Outerspace Conference*, Fermilab, May 1999.
- [49] Parameters of the Preliminary Reference Earth Model are given by A. Dziewonski, Earth Structure, Global, in: “The Encyclopedia of Solid Earth Geophysics”, D. E. James (Ed), (Van Nostrand Reinhold, New York, 1989) p. 331; also see R. Gandhi, C. Quigg, M. Hall Reno, and I. Sarcevic, Astroparticle Physics **5**, 81 (1996).
- [50] R. Bernstein and S. Parke, Phys. Rev. **D44**, 2069 (1991).
- [51] E. Akhmedov, P. Lipari, and M. Lusignoli, Phys. Lett. **B300**, 128 (1993); P. Lipari and M. Lusignoli, Phys. Rev. **D58**, 073005 (1998); E. Akhmedov, A. Dighe, P. Lipari, and A.Yu. Smirnov, Nucl. Phys. **B542**, 3 (1999).
- [52] S.T. Petcov, Phys. Lett. **B434**, 321 (1998); M.V. Chizhov, M. Maris, and S.T. Petcov, hep-ph/9810501; M.V. Chizhov and S.T. Petcov, hep-ph/9903424.
- [53] H.W. Zaglauer and K.H. Schwarzer, Z. Phys. **C40**, 273 (1988); Q. Liu, S. Mikheyev, and A.Yu. Smirnov, Phys. Lett. **B440**, 319 (1998); E.K. Akhmedov, Nucl. Phys. **B538**, 25 (1998); P.I. Krastev, Nuovo Cimento A **103**, 361 (1990).
- [54] J. Pruet and G.M. Fuller, astro-ph/9904023.
- [55] J. Pantaleone, Phys. Rev. **D49**, 2152 (1994); Phys. Rev. Lett. **81**, 5060 (1998).
- [56] V. Barger, N. Deshpande, P.B. Pal, R.J.N. Phillips, and K. Whisnant, Phys. Rev. **D43**, 1759 (1991).
- [57] L.J. Hall and H. Murayama, Phys. Lett. **B436**, 323 (1998); hep-ph/9810468.
- [58] F. Vissani and A.Yu. Smirnov, Phys. Lett. **B432**, 376 (1998).
- [59] KARMEN collaboration, K. Eitel and B. Zeitnitz, talk presented at *Neutrino-98*, Takayama, Japan, June 1998, hep-ex/9809007; M. Mezzetto, talk presented at *The 8th International Workshop on Neutrino Telescopes*, Venice, Italy, Feb. 1999.
- [60] J.N. Bahcall, P. Krastev, and A.Yu. Smirnov, Phys. Rev. **D58**, 096016 (1998).
- [61] J.N. Bahcall, P. Krastev, and A.Yu. Smirnov, hep-ph/9905220.
- [62] M.C. Gonzalez-Garcia, P.C. de Holanda, C. Peña-Garay, and J.W.F. Valle, hep-ph/9906469.
- [63] V. Barger, K. Whisnant, and R.J.N. Phillips, Phys. Rev. **D 24**, 538 (1981); S.L. Glashow and L.M. Krauss, Phys. Lett. **B190**, 199 (1987).
- [64] E. Church et al. (BooNE Collab.), “A letter of intent for an experiment to measure  $\nu_\mu \rightarrow \nu_e$  oscillations and  $\nu_\mu$  disappearance at the Fermilab Booster”, May 16, 1997, unpublished.

TABLE I. Neutrino and antineutrino fluxes calculated for the baseline lengths  $L = 7332$  km (FNAL  $\rightarrow$  Gran Sasso) and  $L = 732$  km (FNAL  $\rightarrow$  Soudan). In the calculation the neutrino fluxes have been averaged over a circular area with radius 1 km (0.1 km) for  $L = 7332$  km (732 km). This averaging provides an approximate model for the  $\mathcal{O}(10\%)$  reduction in the neutrino fluxes at the far site due to the finite divergence of the parent muon beam in the straight section of the storage ring.

parent	$E_\mu$ (GeV)	10	20	50	250
FNAL $\rightarrow$ Soudan					
$\mu^-$	$\nu_\mu$ ( $10^{12} m^{-2} yr^{-1}$ )	0.79	3.3	21	460
$\mu^-$	$\bar{\nu}_e$ ( $10^{12} m^{-2} yr^{-1}$ )	0.79	3.3	21	470
$\mu^+$	$\nu_e$ ( $10^{12} m^{-2} yr^{-1}$ )	0.85	3.3	21	470
$\mu^+$	$\bar{\nu}_\mu$ ( $10^{12} m^{-2} yr^{-1}$ )	0.84	3.3	21	470
FNAL $\rightarrow$ Gran Sasso					
$\mu^-$	$\nu_\mu$ ( $10^{10} m^{-2} yr^{-1}$ )	0.79	3.3	21	470
$\mu^-$	$\bar{\nu}_e$ ( $10^{10} m^{-2} yr^{-1}$ )	0.79	3.3	21	470
$\mu^+$	$\nu_e$ ( $10^{10} m^{-2} yr^{-1}$ )	0.83	3.3	21	470
$\mu^+$	$\bar{\nu}_\mu$ ( $10^{10} m^{-2} yr^{-1}$ )	0.85	3.3	21	470

TABLE II. Neutrino and antineutrino CC interaction rates in the absence of oscillations, calculated for the baseline lengths  $L = 7332$  km (FNAL  $\rightarrow$  Gran Sasso) and  $L = 732$  km (FNAL  $\rightarrow$  Soudan). In the calculation the neutrino fluxes have been averaged over a circular area with radius 1 km (0.1 km) for  $L = 7332$  km (732 km). This averaging provides an approximate model for the  $\mathcal{O}(10\%)$  reduction in the neutrino fluxes at the far site due to the finite divergence of the parent muon beam in the straight section of the storage ring.

parent	$E_\mu$ (GeV)	10	20	50	250
FNAL $\rightarrow$ Soudan					
$\mu^-$	$\nu_\mu$ (per kt-yr)	$2.2 \times 10^3$	$1.9 \times 10^4$	$2.9 \times 10^5$	$3.1 \times 10^7$
$\mu^-$	$\bar{\nu}_e$ (per kt-yr)	$9.6 \times 10^2$	$8.0 \times 10^3$	$1.3 \times 10^5$	$1.4 \times 10^7$
$\mu^+$	$\nu_e$ (per kt-yr)	$1.9 \times 10^3$	$1.6 \times 10^4$	$2.4 \times 10^5$	$2.7 \times 10^7$
$\mu^+$	$\bar{\nu}_\mu$ (per kt-yr)	$1.2 \times 10^3$	$9.5 \times 10^3$	$1.5 \times 10^5$	$1.6 \times 10^7$
FNAL $\rightarrow$ Gran Sasso					
$\mu^-$	$\nu_\mu$ (per kt-yr)	22	$1.9 \times 10^2$	$2.9 \times 10^3$	$3.1 \times 10^5$
$\mu^-$	$\bar{\nu}_e$ (per kt-yr)	9.5	80	$1.3 \times 10^3$	$1.4 \times 10^5$
$\mu^+$	$\nu_e$ (per kt-yr)	20	$1.6 \times 10^2$	$2.4 \times 10^3$	$2.7 \times 10^5$
$\mu^+$	$\bar{\nu}_\mu$ (per kt-yr)	12	94	$1.5 \times 10^3$	$1.6 \times 10^5$

TABLE III. Muon neutrino and electron antineutrino CC interaction rates in the absence of oscillations, calculated for baseline length  $L = 732$  km (FNAL  $\rightarrow$  Soudan), for MINOS using the wide band beam and a muon storage ring with  $E_\mu = 10, 20, 50$  and 250 GeV.

Experiment		$\langle E_{\nu_\mu} \rangle$ (GeV)	$\langle E_{\bar{\nu}_e} \rangle$ (GeV)	N( $\nu_\mu$ CC) (per kt-yr)	N( $\bar{\nu}_e$ CC) (per kt-yr)
MINOS	Beam				
	Low energy	3	–	458	1.3
	Medium energy	6	–	1439	0.9
	High energy	12	–	3207	0.9
Muon ring	$E_\mu$ (GeV)				
	10	7	6	2200	960
	20	14	12	19000	8000
	50	35	30	$2.9 \times 10^5$	$1.3 \times 10^5$
	250	175	150	$3.1 \times 10^7$	$1.4 \times 10^7$

TABLE IV. Tilt angle, distance, and average electron density for long-baseline experiments with neutrino source at Fermilab.

Detector site	Tilt angle (degrees)	$L$ (km)	$\langle N_e \rangle$ ( $N_0/\text{cm}^3$ )	$L_{core}$ (km)	$\langle N_e \rangle_{mantle}$ ( $N_0/\text{cm}^3$ )	$\langle N_e \rangle_{core}$ ( $N_0/\text{cm}^3$ )
Soudan	3.3	732	1.67	0	1.67	–
Gran Sasso	35	7332	2.09	0	2.09	–
Kamioka	46	9160	2.26	0	2.26	–
South Pole	67	11700	3.39	4640	2.33	4.99



TABLE V. Muon neutrino CC interaction rates calculated for a distance  $L$  downstream of a storage ring containing unpolarized negative muons. The event rates assume  $\nu_\mu \rightarrow \nu_\tau$  oscillations with  $\sin^2 2\theta = 1$ . Results for  $\nu_\mu \rightarrow \nu_s$  oscillations are shown in parentheses for  $L = 7332$  km; for  $L = 732$  km matter effects are small and the results for  $\nu_\mu \rightarrow \nu_\tau$  and  $\nu_\mu \rightarrow \nu_s$  are very similar. Also shown are the tau neutrino CC interaction rates due to  $\nu_\mu \rightarrow \nu_\tau$  oscillations.

$E_\mu$ (GeV)	$L$ (km)	$\Delta m^2$ (eV <sup>2</sup> /c <sup>4</sup> )	$\langle P \rangle$ $\nu_\mu \rightarrow \nu_\tau$ ( $\nu_\mu \rightarrow \nu_s$ )	N( $\nu_\mu$ CC) (per 10 kt-yr)	Significance	N( $\nu_\tau$ CC) (per kt-yr)
10	7332	0	0 (0)	220 (220)	0 (0)	0
10	7332	0.002	0.53 (0.18)	100 (180)	12 $\sigma$ (3.0 $\sigma$ )	1.9
10	7332	0.003	0.29 (0.36)	160 (140)	5.2 $\sigma$ (6.7 $\sigma$ )	0.7
10	7332	0.004	0.63 (0.64)	80 ( 80)	15 $\sigma$ (16 $\sigma$ )	2.1
10	7332	0.005	0.56 (0.48)	100 (120)	12 $\sigma$ (9.9 $\sigma$ )	1.9
10	7332	0.006	0.38 (0.37)	140 (140)	7.1 $\sigma$ (7.0 $\sigma$ )	1.2
20	7332	0	0 (0)	1900 (1900)	0 (0)	0
20	7332	0.002	0.80 (0.27)	370 (1370)	78 $\sigma$ (14 $\sigma$ )	43
20	7332	0.003	0.81 (0.25)	360 (1400)	80 $\sigma$ (12 $\sigma$ )	46
20	7332	0.004	0.53 (0.18)	880 (1530)	34 $\sigma$ (8.6 $\sigma$ )	30
20	7332	0.005	0.30 (0.21)	1310 (1480)	15 $\sigma$ (10 $\sigma$ )	15
20	7332	0.006	0.29 (0.36)	1320 (1190)	15 $\sigma$ (20 $\sigma$ )	14
50	7332	0	0 (0)	28800 (28800)	0 (0)	0
50	7332	0.002	0.26 (0.10)	21300 (25900)	52 $\sigma$ (18 $\sigma$ )	350
50	7332	0.003	0.48 (0.18)	15000 (23700)	110 $\sigma$ (33 $\sigma$ )	660
50	7332	0.004	0.67 (0.24)	9500 (22000)	200 $\sigma$ (46 $\sigma$ )	950
50	7332	0.005	0.80 (0.27)	5700 (21000)	310 $\sigma$ (54 $\sigma$ )	1160
50	7332	0.006	0.86 (0.28)	4200 (20800)	380 $\sigma$ (55 $\sigma$ )	1260
10	732	0	0	22200	0	0
10	732	0.002	0.08	20500	12 $\sigma$	20
10	732	0.003	0.16	18700	26 $\sigma$	43
10	732	0.004	0.26	16500	45 $\sigma$	74
10	732	0.005	0.37	14100	69 $\sigma$	110
10	732	0.006	0.47	11700	98 $\sigma$	150
20	732	0	0	185000	0	0
20	732	0.002	0.020	181000	8.6 $\sigma$	89
20	732	0.003	0.044	177000	19 $\sigma$	200
20	732	0.004	0.076	171000	34 $\sigma$	350
20	732	0.005	0.11	164000	52 $\sigma$	530
20	732	0.006	0.16	156000	74 $\sigma$	750
50	732	0	0	$2.88 \times 10^6$	0	0
50	732	0.002	$3.3 \times 10^{-3}$	$2.88 \times 10^6$	5.6 $\sigma$	410
50	732	0.003	$7.4 \times 10^{-3}$	$2.86 \times 10^6$	13 $\sigma$	910
50	732	0.004	0.013	$2.84 \times 10^6$	22 $\sigma$	1600
50	732	0.005	0.020	$2.83 \times 10^6$	35 $\sigma$	2500
50	732	0.006	0.029	$2.81 \times 10^6$	50 $\sigma$	3600
250	732	0	0	$3.11 \times 10^8$	0	0
250	732	0.002	$1.4 \times 10^{-4}$	$3.11 \times 10^8$	2.5 $\sigma$	3000
250	732	0.003	$3.2 \times 10^{-4}$	$3.11 \times 10^8$	5.7 $\sigma$	6800
250	732	0.004	$5.8 \times 10^{-4}$	$3.11 \times 10^8$	10 $\sigma$	12100
250	732	0.005	$9.0 \times 10^{-4}$	$3.11 \times 10^8$	16 $\sigma$	18900
250	732	0.006	$1.3 \times 10^{-3}$	$3.11 \times 10^8$	23 $\sigma$	27200

TABLE VI. Average  $\nu_e \rightarrow \nu_\mu$  and  $\bar{\nu}_e \rightarrow \bar{\nu}_\mu$  oscillation probabilities, and muon neutrino and antineutrino CC interaction rates for a detector  $L = 7332$  km downstream of a storage ring containing unpolarized muons. The event rates assume  $\nu_e \rightarrow \nu_\mu$  oscillations with  $\sin^2 2\theta = 0.1$ . Also shown is the average oscillation probability for  $\nu_e \rightarrow \nu_\mu$ , assuming no matter effects; the probability for  $\bar{\nu}_e \rightarrow \bar{\nu}_\mu$  without matter effects is the same as for  $\nu_e \rightarrow \nu_\mu$ .

$E_\mu$ (GeV)	$\Delta m^2$ (eV <sup>2</sup> /c <sup>4</sup> )	$\langle P(\nu_e \rightarrow \nu_\mu) \rangle$	N( $\nu_\mu$ CC) (per 10 kt-yr)	$\langle P(\bar{\nu}_e \rightarrow \bar{\nu}_\mu) \rangle$	N( $\bar{\nu}_\mu$ CC) (per 10 kt-yr)	No matter effects $\langle P(\nu_e \rightarrow \nu_\mu) \rangle$
10	0.002	0.46	90	0.015	1.4	0.041
10	0.003	0.53	110	0.019	1.8	0.042
10	0.004	0.27	55	0.032	3.0	0.061
10	0.005	0.10	20	0.031	2.9	0.047
10	0.006	0.087	18	0.030	2.9	0.046
20	0.002	0.11	170	0.011	8.8	0.082
20	0.003	0.29	460	0.016	13	0.069
20	0.004	0.46	730	0.015	12	0.041
20	0.005	0.55	870	0.014	11	0.032
20	0.006	0.53	840	0.019	15	0.042
50	0.002	0.0067	170	0.0016	21	0.033
50	0.003	0.025	630	0.0044	57	0.057
50	0.004	0.059	1480	0.0079	110	0.074
50	0.005	0.11	2750	0.011	140	0.082
50	0.006	0.18	4380	0.014	180	0.082

TABLE VII. Electron neutrino CC interaction rates calculated for a distance  $L$  downstream of a storage ring containing unpolarized positive muons assuming  $\nu_e \rightarrow \nu_\tau$  oscillations with  $\sin^2 2\theta = 0.1$ . Also shown are the tau neutrino CC interaction rates due to oscillations.

$E_\mu$ (GeV)	$L$ (km)	$\Delta m^2$ ( $eV^2/c^4$ )	$\langle P \rangle$	$N(\nu_e \text{ CC})$ (per 10 kt-yr)	Significance	$N(\nu_\tau \text{ CC})$ (per kt-yr)
10	7332	0	0	200	0	0
10	7332	0.002	0.46	110	$8.9\sigma$	1.1
10	7332	0.003	0.53	95	$11\sigma$	1.6
10	7332	0.004	0.27	150	$4.5\sigma$	0.9
10	7332	0.005	0.10	180	$1.5\sigma$	0.3
10	7332	0.006	0.087	180	$1.3\sigma$	0.2
20	7332	0	0	1580	0	0
20	7332	0.002	0.11	1410	$4.5\sigma$	7.2
20	7332	0.003	0.29	1120	$14\sigma$	14
20	7332	0.004	0.46	850	$25\sigma$	17
20	7332	0.005	0.55	710	$33\sigma$	16
20	7332	0.006	0.53	740	$31\sigma$	16
50	7332	0	0	24100	0	0
50	7332	0.002	0.007	24000	$1.0\sigma$	4.2
50	7332	0.003	0.026	23000	$3.9\sigma$	19
50	7332	0.004	0.062	22100	$9.8\sigma$	51
50	7332	0.005	0.12	20900	$19\sigma$	100
50	7332	0.006	0.18	19300	$31\sigma$	170
10	732	0	0	19400	0	0
10	732	0.002	0.010	19200	$1.4\sigma$	1.7
10	732	0.003	0.021	19000	$3.0\sigma$	3.7
10	732	0.004	0.033	18800	$4.7\sigma$	6.3
10	732	0.005	0.045	18500	$6.4\sigma$	9.2
10	732	0.006	0.057	18300	$8.2\sigma$	12
20	732	0	0	156000	0	0
20	732	0.002	0.0028	156000	$1.1\sigma$	8.8
20	732	0.003	0.0060	155000	$2.4\sigma$	20
20	732	0.004	0.010	154000	$4.0\sigma$	34
20	732	0.005	0.015	154000	$6.0\sigma$	52
20	732	0.006	0.021	153000	$8.3\sigma$	73
50	732	0	0	$2.37 \times 10^6$	0	0
50	732	0.002	$5 \times 10^{-4}$	$2.37 \times 10^6$	$0.7\sigma$	42
50	732	0.003	$1 \times 10^{-3}$	$2.37 \times 10^6$	$1.6\sigma$	95
50	732	0.004	$2 \times 10^{-3}$	$2.37 \times 10^6$	$2.8\sigma$	170
50	732	0.005	$3 \times 10^{-3}$	$2.36 \times 10^6$	$4.4\sigma$	260
50	732	0.006	$4 \times 10^{-3}$	$2.36 \times 10^6$	$6.3\sigma$	380
250	732	0	0	$2.73 \times 10^8$	0	0
250	732	0.002	$2 \times 10^{-5}$	$2.73 \times 10^8$	$0.3\sigma$	360
250	732	0.003	$5 \times 10^{-5}$	$2.73 \times 10^8$	$0.8\sigma$	810
250	732	0.004	$8 \times 10^{-5}$	$2.73 \times 10^8$	$1.3\sigma$	1400
250	732	0.005	$1 \times 10^{-4}$	$2.73 \times 10^8$	$2.1\sigma$	2300
250	732	0.006	$2 \times 10^{-4}$	$2.73 \times 10^8$	$3.0\sigma$	3200

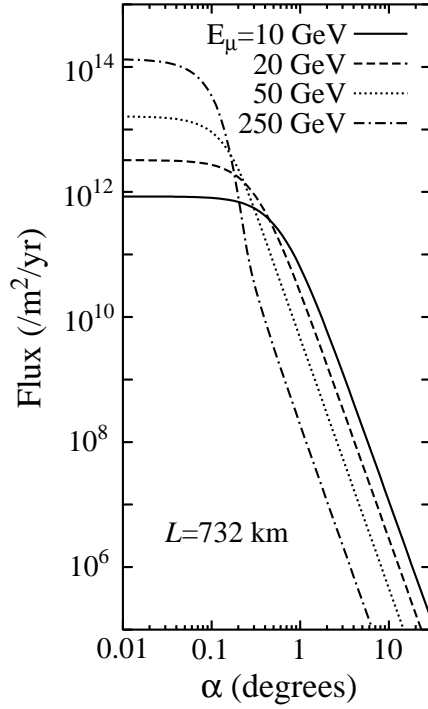


FIG. 1. Total neutrino flux of a given flavor versus angle at the source from the beamline at  $L = 732$  km for  $E_\mu = 10$  GeV (solid line), 20 GeV (dashed), 50 GeV (dotted), and 250 GeV (dot-dashed), assuming  $1.6 \times 10^{20}$  neutrinos in the beam per operational year. A Gaussian muon beam divergence of 1 mrad has been folded in. The total antineutrino flux is the same.

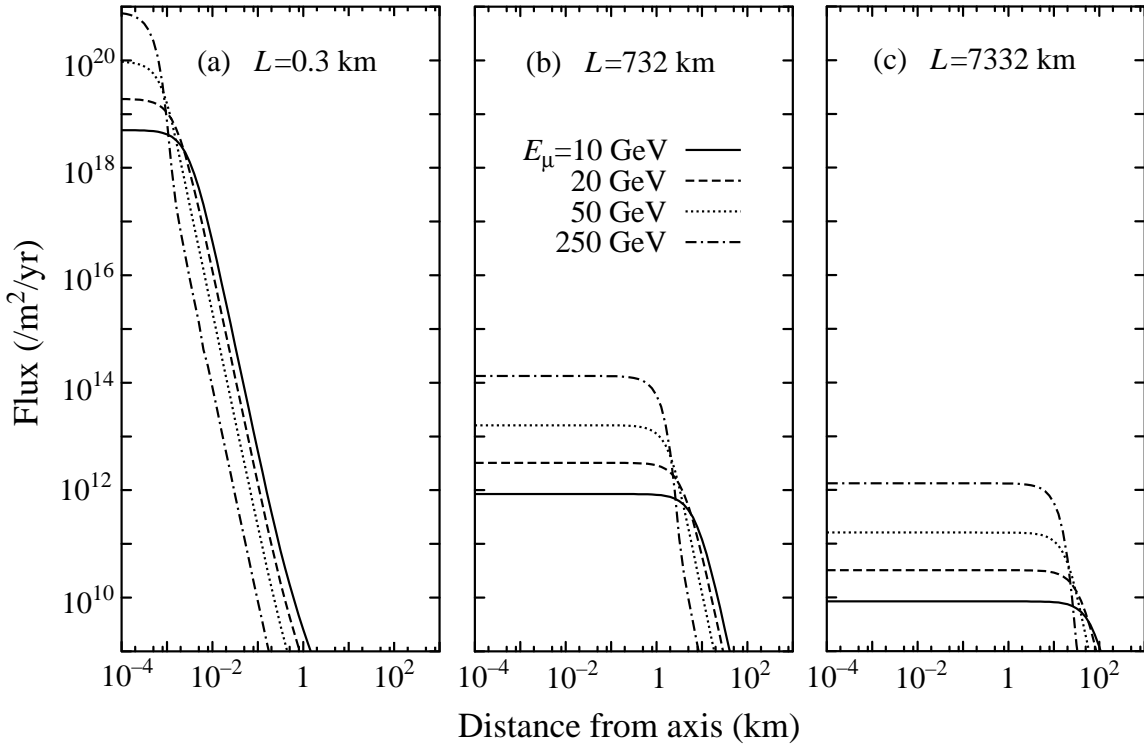


FIG. 2. Total neutrino flux of a given flavor versus perpendicular distance from the beam axis at (a)  $L = 0.3$  km, (b) 732 km, and (c) 7332 km (dotted) for  $E_\mu = 10$  GeV (solid line), 20 GeV (dashed), 50 GeV (dotted), and 250 GeV (dot-dashed), assuming  $1.6 \times 10^{20}$  neutrinos in the beam per operational year. A Gaussian muon beam divergence of 1 mrad has been folded in. The total antineutrino flux is the same.

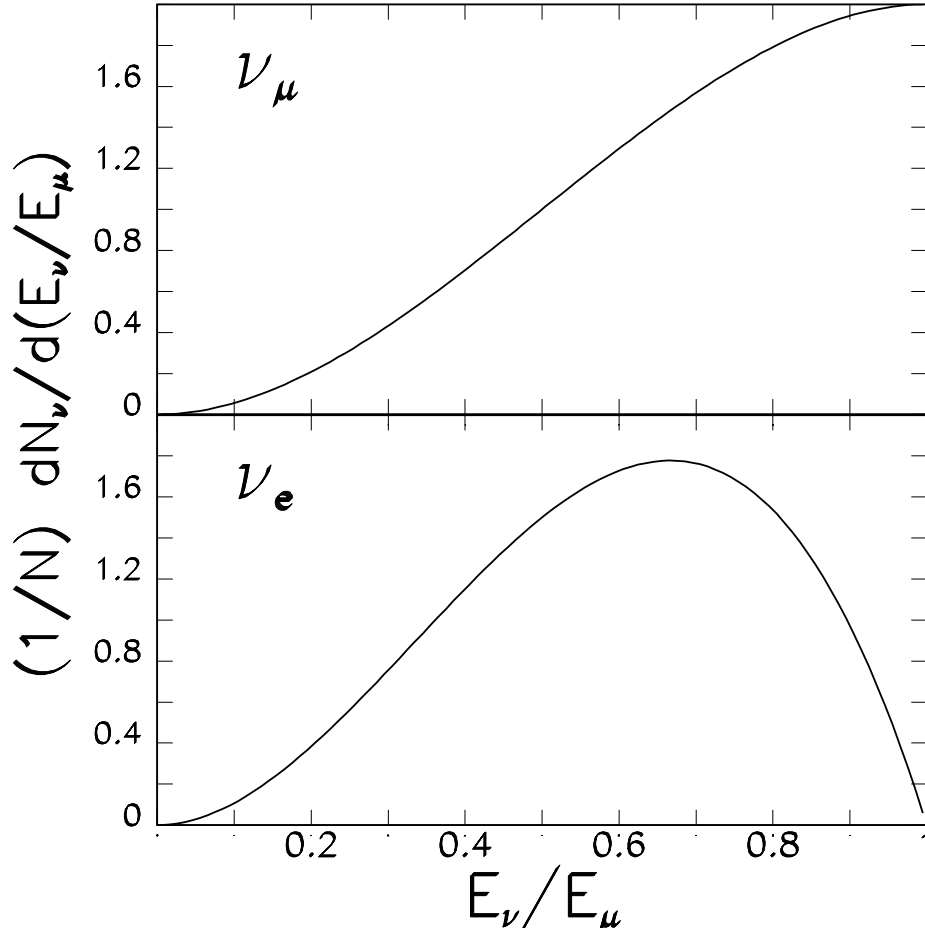


FIG. 3. Neutrino and antineutrino spectra for muon-type neutrinos (top) and electron-type neutrinos (bottom) in the beam downstream of a muon storage ring neutrino source containing unpolarized muons.

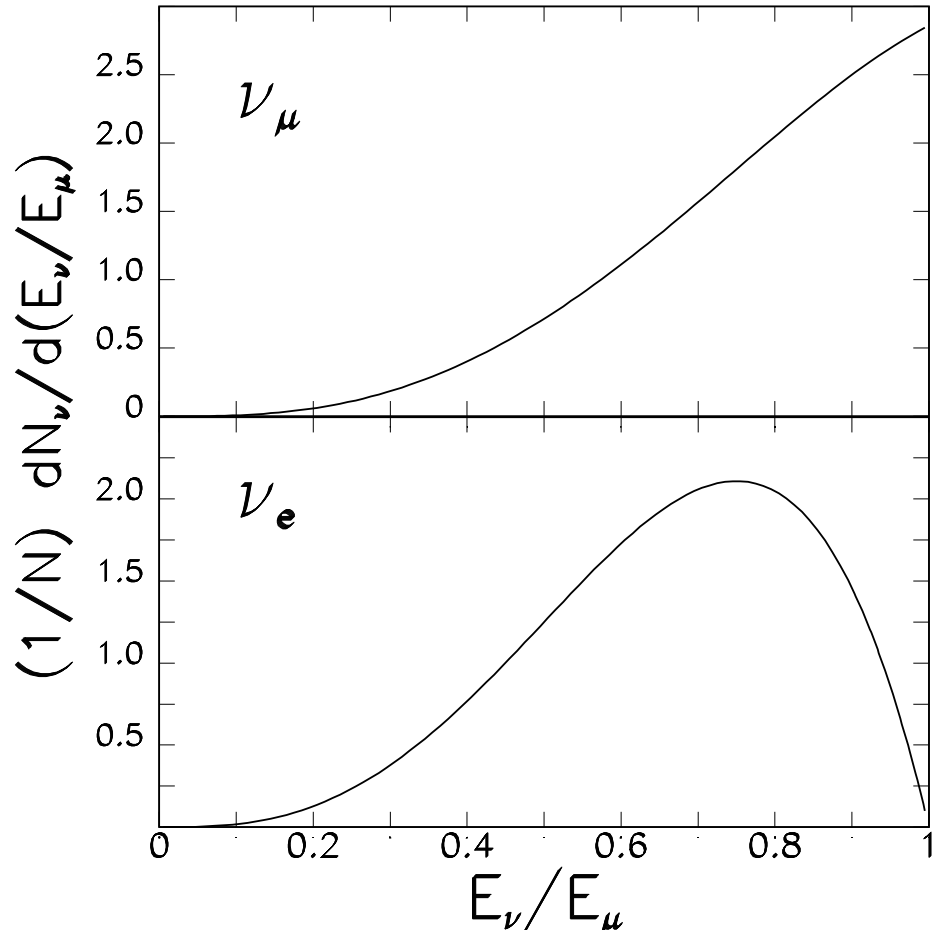


FIG. 4. Event energy distributions for the CC interactions of muon-type neutrinos (top) and electron-type neutrinos (bottom) downstream of a muon storage ring neutrino source containing unpolarized muons.

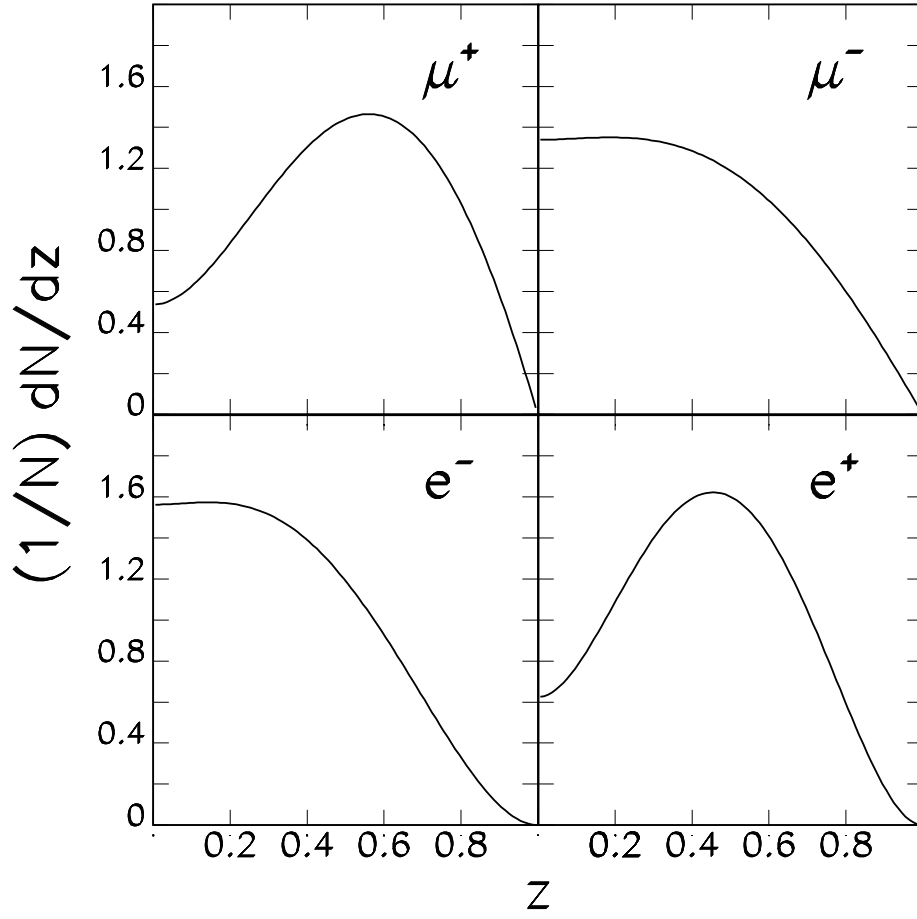


FIG. 5. Lepton energy spectra for CC  $\bar{\nu}_\mu$  (top left),  $\nu_\mu$  (top right),  $\nu_e$  (bottom left), and  $\bar{\nu}_e$  (bottom right) interactions.

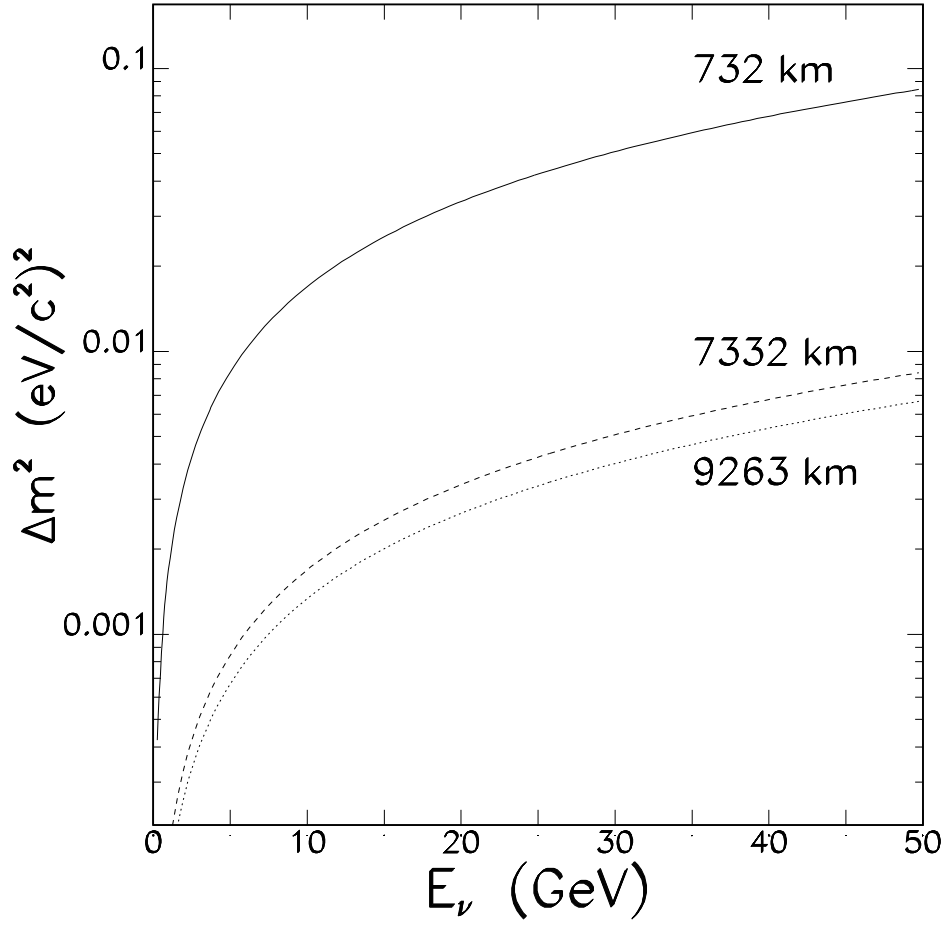


FIG. 6. The  $\Delta m^2$  in Eq. 17 that yields a maximum vacuum oscillation probability, shown versus the neutrino energy for three baseline lengths: (i) Fermilab  $\rightarrow$  Soudan (solid line), (ii) Fermilab  $\rightarrow$  Gran Sasso (broken line), and (iii) Fermilab  $\rightarrow$  Kamioka Mine (dotted line).



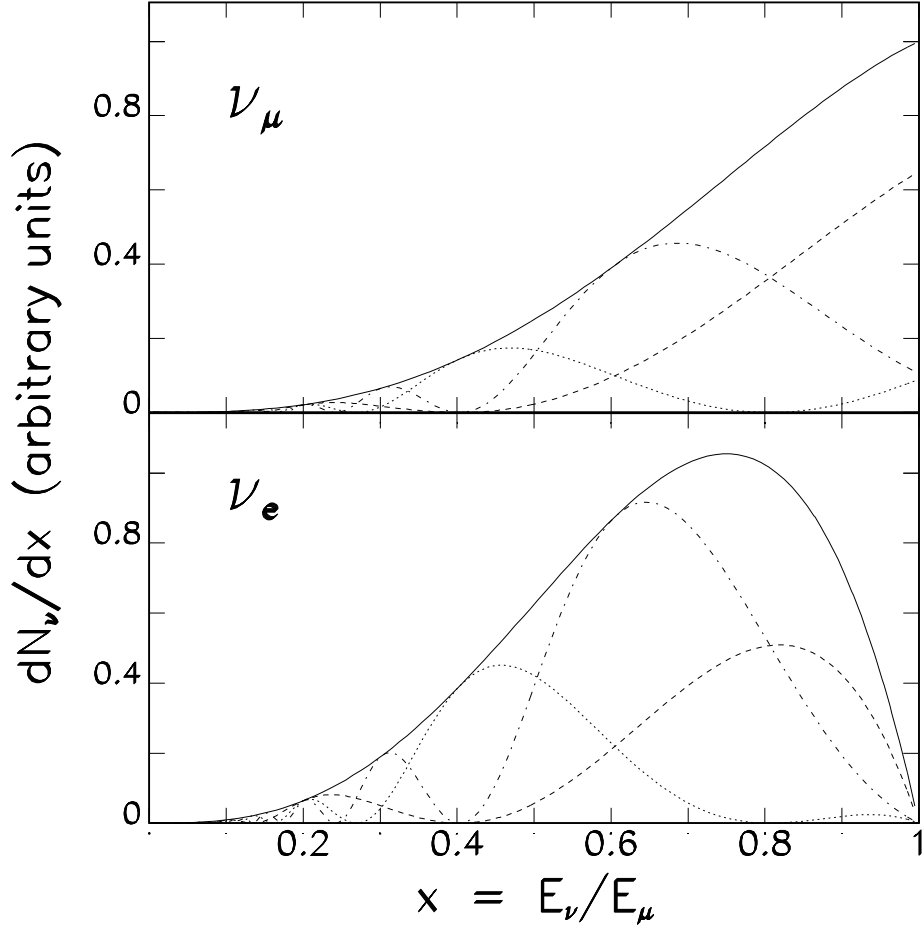


FIG. 7. Neutrino and antineutrino charged current interaction spectra for muon-type neutrinos (top) and electron-type neutrinos (bottom) downstream of a muon storage ring neutrino source containing unpolarized muons. The differential distributions are shown as a function of the parameter  $\eta \equiv \Delta m^2 L/E_\mu$  for  $\eta = 0.5$  (broken curves),  $\eta = 1$  (dotted curves), and  $\eta = 1.5$  (dot-dashed curves). The solid curves show the spectra in the absence of oscillations.

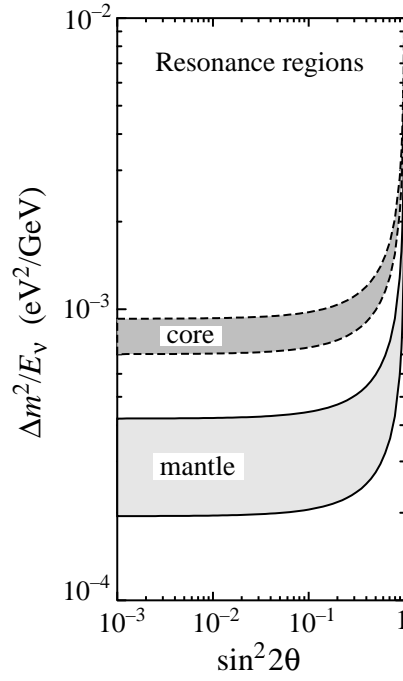


FIG. 8. Regions of  $\Delta m^2/E_\nu$  versus  $\sin^2 2\theta$  which have maximal mixing in matter in the Earth. The range of  $\Delta m^2/E_\nu$  values is due to the variation of the density in the mantle and the core.

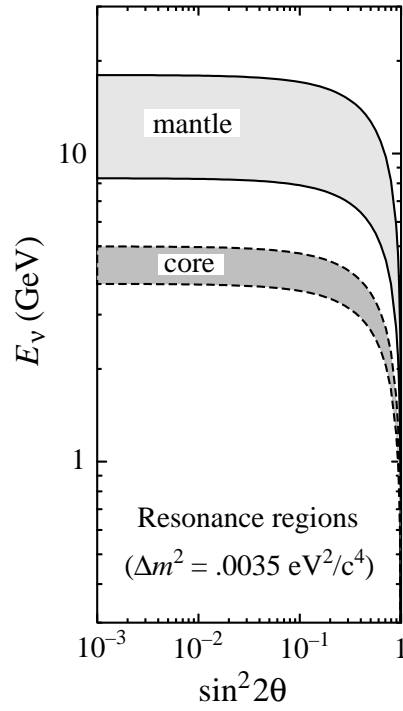


FIG. 9. Regions of  $E_\nu$  versus  $\sin^2 2\theta$  which have maximal mixing in matter in the Earth for  $\Delta m^2 = 3.5 \times 10^{-3} \text{ eV}^2/c^4$ . The range of  $E_\nu$  values is due to the variation of the density in the mantle and the core.

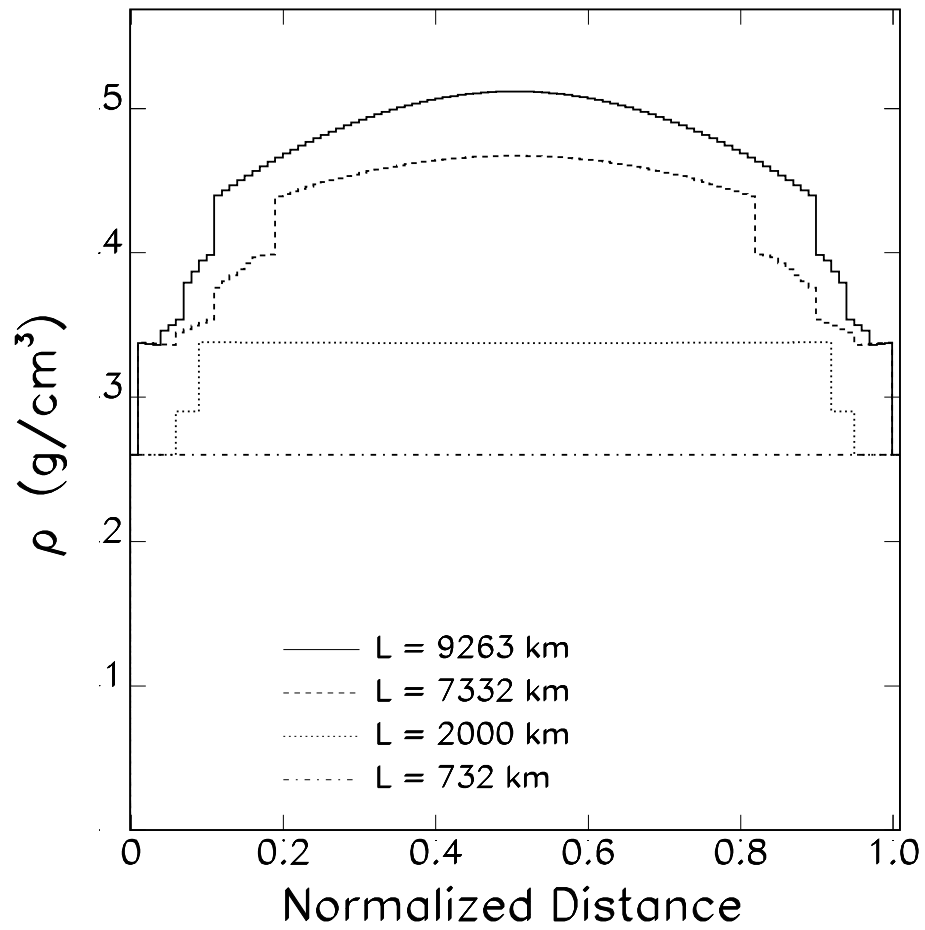


FIG. 10. Density profiles along a selection of chords of length  $L$  passing through the Earth; the horizontal axis is the fraction of the total path length.

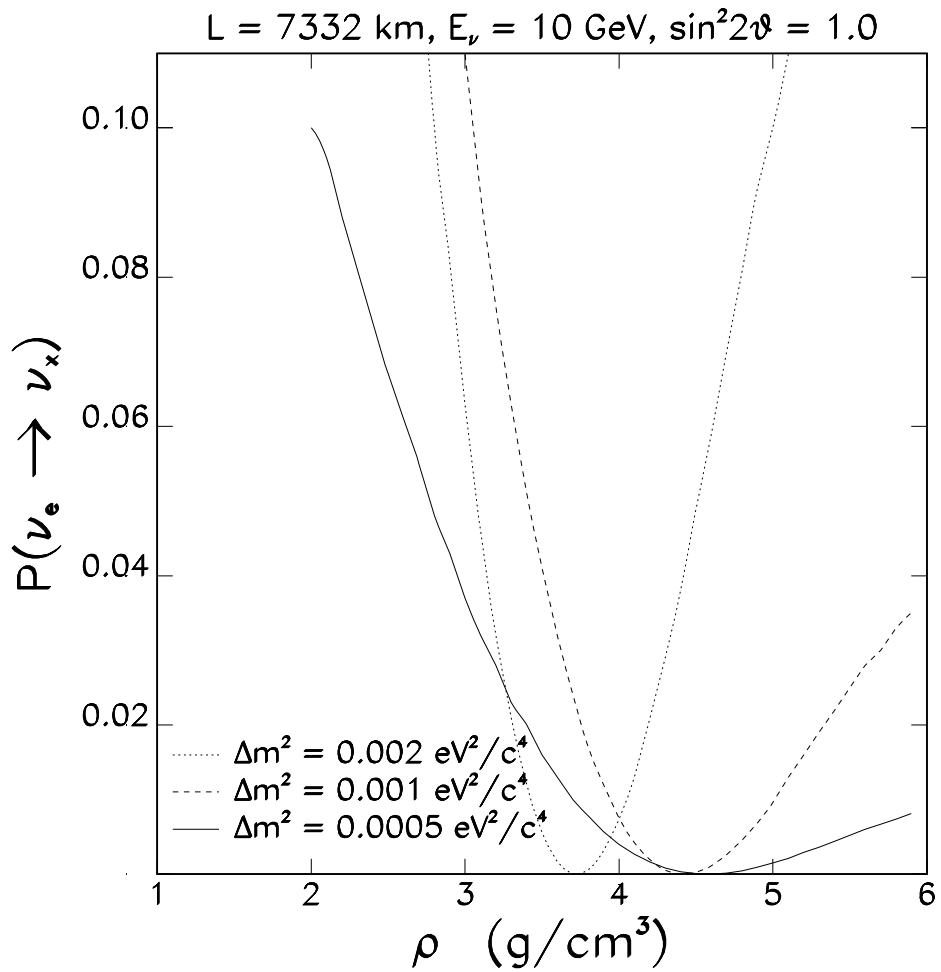


FIG. 11. Electron neutrino disappearance probability  $P(\nu_e \rightarrow \nu_x)$  for  $x = \mu$  or  $\tau$ , shown as a function of the assumed matter density for 10 GeV electron neutrinos propagating 7332 km through the Earth. The curves correspond to the oscillation parameters  $\sin^2 2\theta = 1$  and  $\Delta m^2$  as indicated.

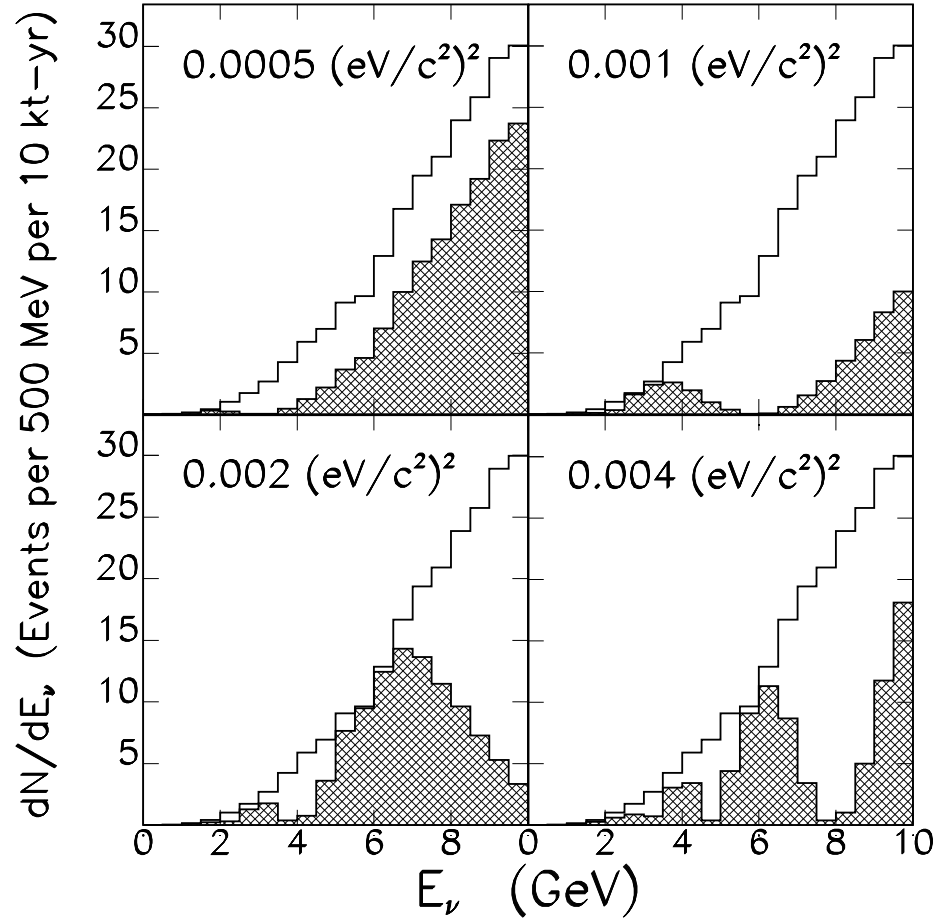


FIG. 12. Modified  $\nu_\mu$  CC interaction spectra for a 10 GeV muon storage ring neutrino source located at FNAL and a detector at the Gran Sasso underground laboratory, shown for several values of the oscillation parameter  $\Delta m^2$ , assuming  $\sin^2 2\theta = 1$ . In each of the four panels the upper curves show the unmodulated spectrum, and the lower curves the modulated spectrum corresponding to the indicated  $\Delta m^2$ .

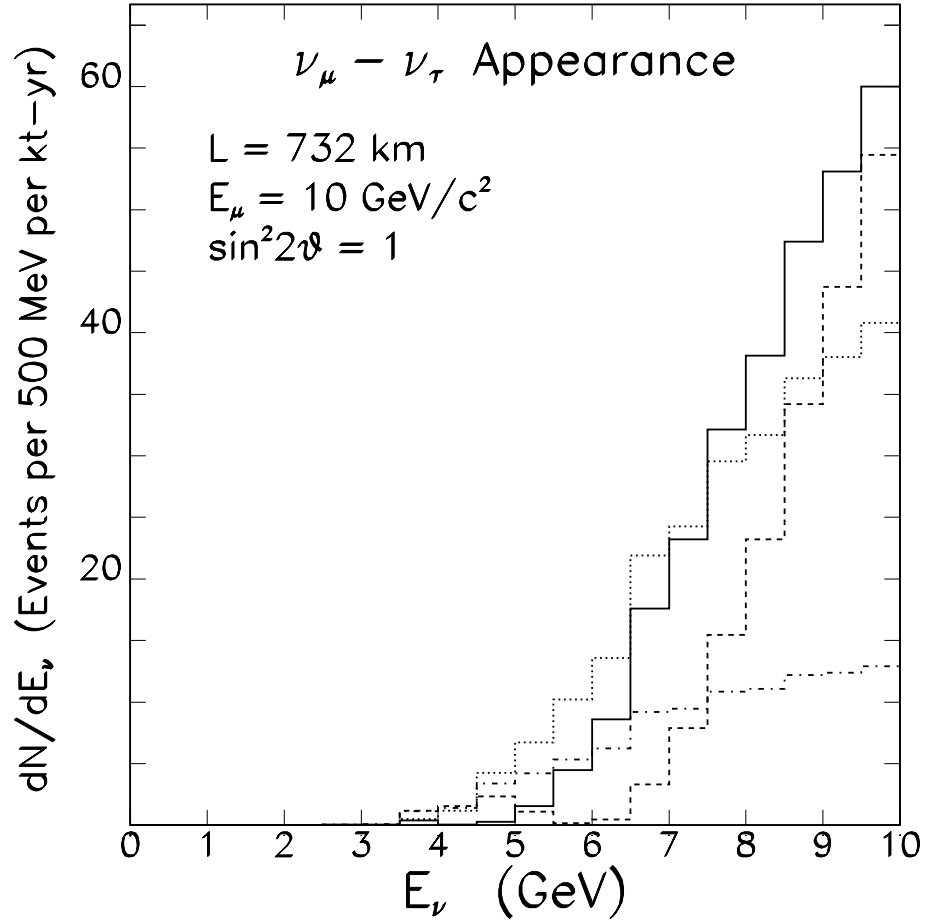


FIG. 13. Predicted  $\nu_\tau$  appearance CC interaction spectra for a 10 GeV muon storage ring neutrino source located at FNAL and a detector at the Soudan mine, shown for several values of the oscillation parameter  $\Delta m^2$ , assuming  $\sin^2 2\theta = 1$ . The curves correspond to  $\Delta m^2 = 0.02 \text{ eV}^2/c^4$  (dotted),  $0.015 \text{ eV}^2/c^4$  (solid),  $0.01 \text{ eV}^2/c^4$  (broken), and  $0.005 \text{ eV}^2/c^4$  (dot-dashed).

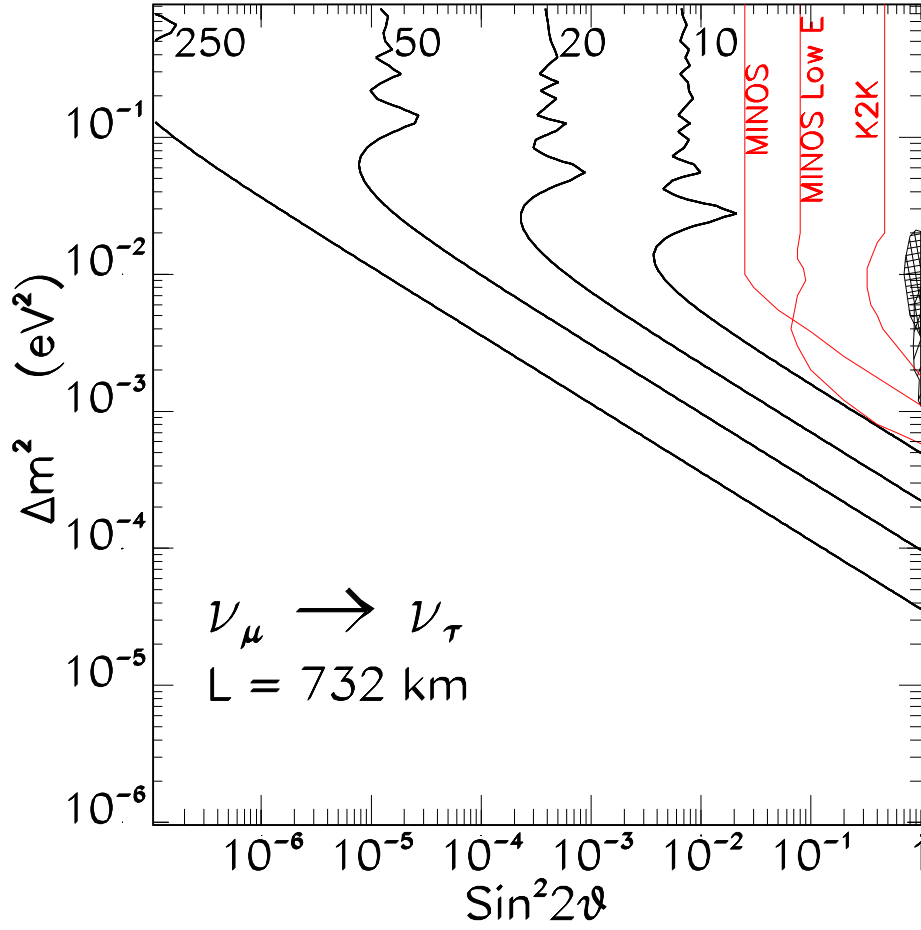


FIG. 14. Single event per kt-yr contours calculated for  $\nu_{\mu} \rightarrow \nu_{\tau}$  appearance 732 km downstream of a muon storage ring neutrino source. From left to right, the contours correspond to unpolarized muons with energies  $E_{\mu} = 250, 50, 20,$  and  $10$  GeV. The shaded areas correspond to the Kamiokande and Super-Kamiokande allowed region of parameter space. Also shown are the expected regions of sensitivity for the MINOS and K2K experiments (as labelled).

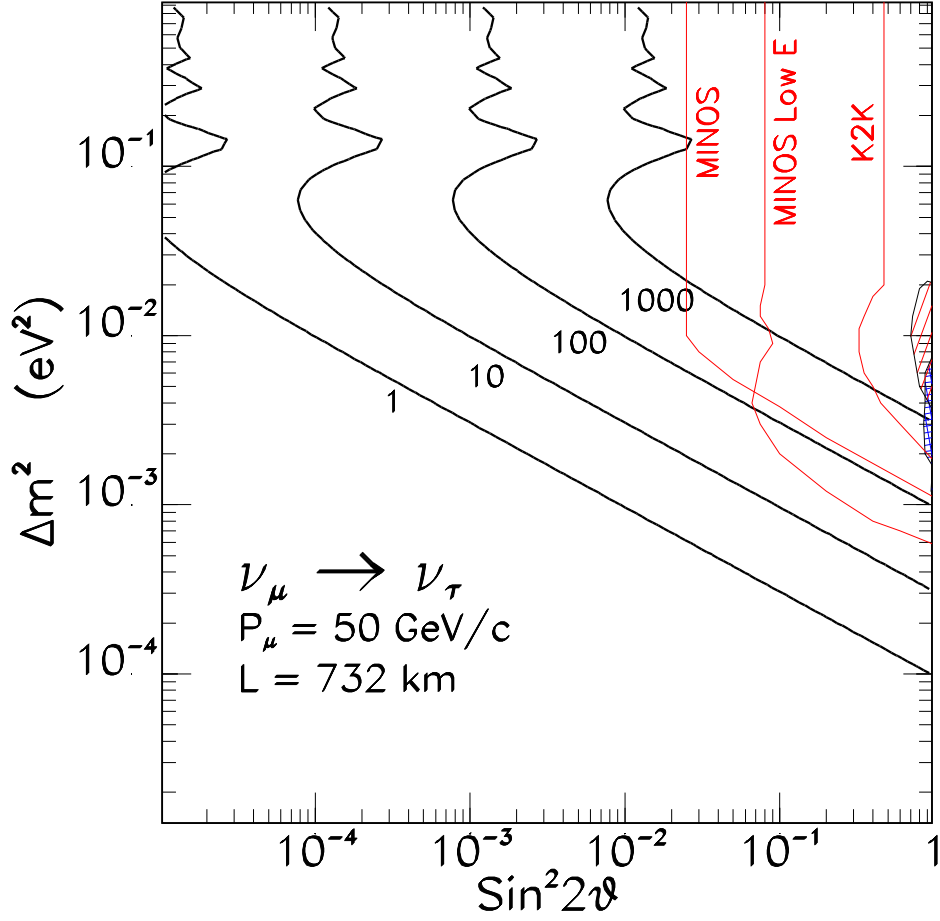


FIG. 15. Contours of constant  $\nu_\tau$  CC interaction event rate for  $\nu_\mu \rightarrow \nu_\tau$  appearance 732 km downstream of a 50 GeV muon storage ring neutrino source. From left to right, the contours correspond to event rates of 1, 10, 100, and 1000 per kt-yr. The shaded areas correspond to the Kamiokande and Super-Kamiokande allowed region of parameter space. Also shown are the expected regions of sensitivity for the MINOS and K2K experiments (as labelled).



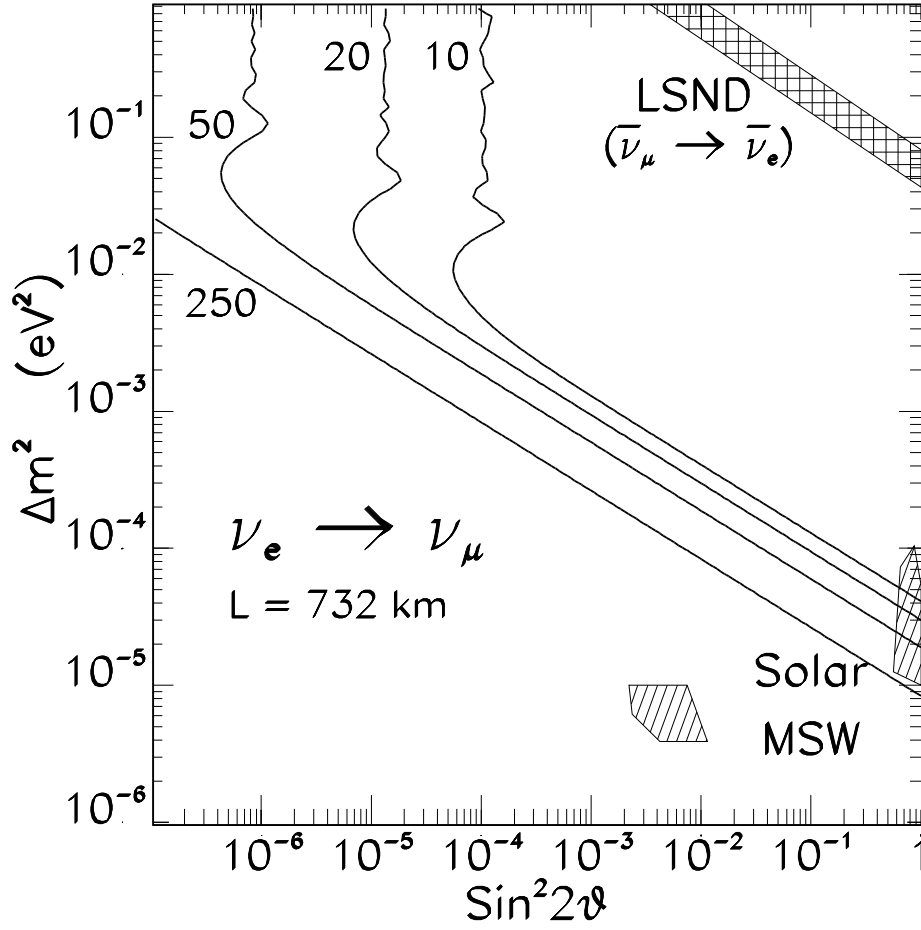


FIG. 16. Single event per 10 kt-yr contours calculated for  $\nu_e \rightarrow \nu_\mu$  appearance 732 km downstream of a muon storage ring neutrino source. From left to right, the contours correspond to unpolarized muons with energies  $E_\mu = 250, 50, 20,$  and  $10$  GeV. The regions favored by the LSND results and the MSW solar neutrino oscillation solutions are also shown.

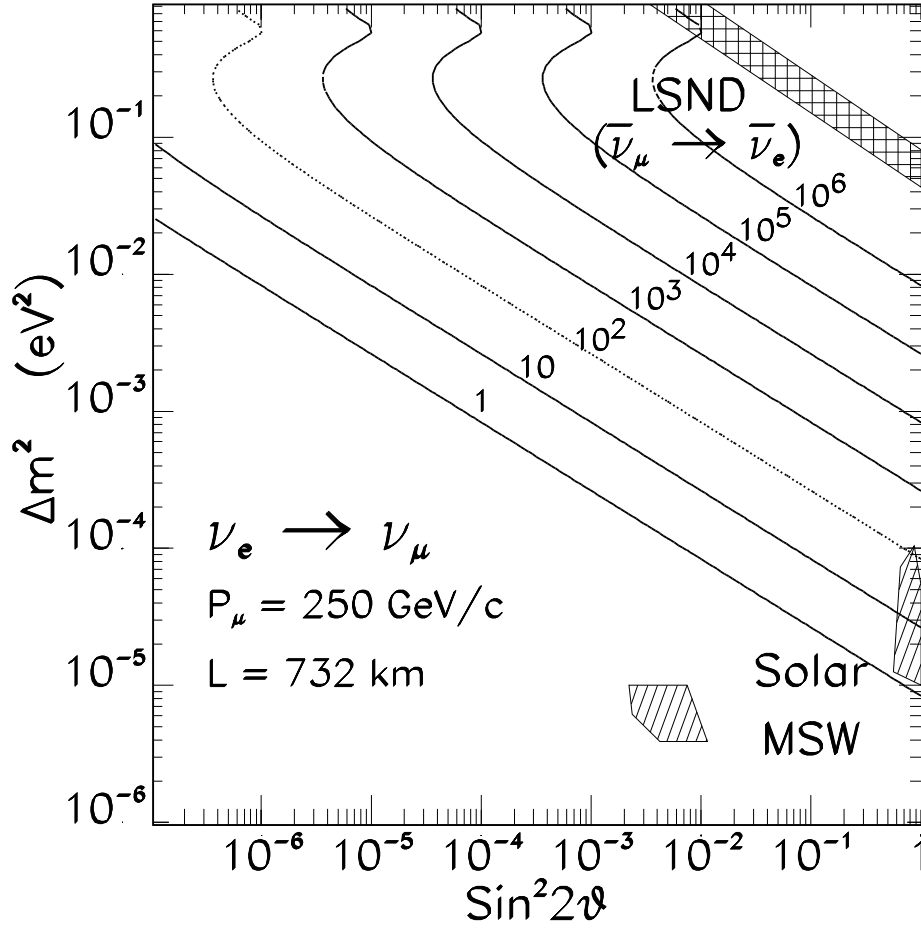


FIG. 17. Contours of constant  $\nu_\mu$  CC interaction event rate for  $\nu_e \rightarrow \nu_\mu$  appearance 732 km downstream of a 250 GeV muon storage ring neutrino source. From left to right, the contours correspond to event rates of 1, 10,  $10^2$ ,  $10^3$ ,  $10^4$ ,  $10^5$  and  $10^6$  per 10 kt-yr. The regions favored by the LSND results and the MSW solar neutrino oscillation solutions are also shown.

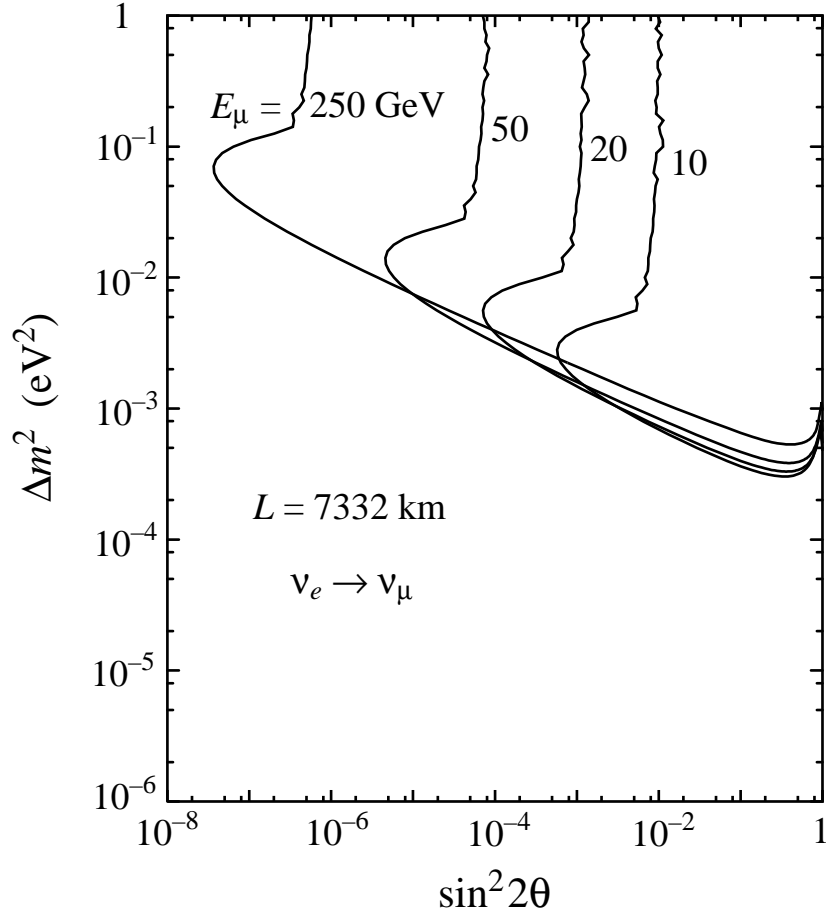


FIG. 18. Single event per 10 kt-yr contours calculated for  $\nu_e \rightarrow \nu_\mu$  appearance 7332 km downstream of a muon storage ring neutrino source, assuming  $\Delta m^2 > 0$ . From left to right, the contours correspond to unpolarized muons with energies  $E_\mu = 250$ , 50, 20, and 10 GeV.

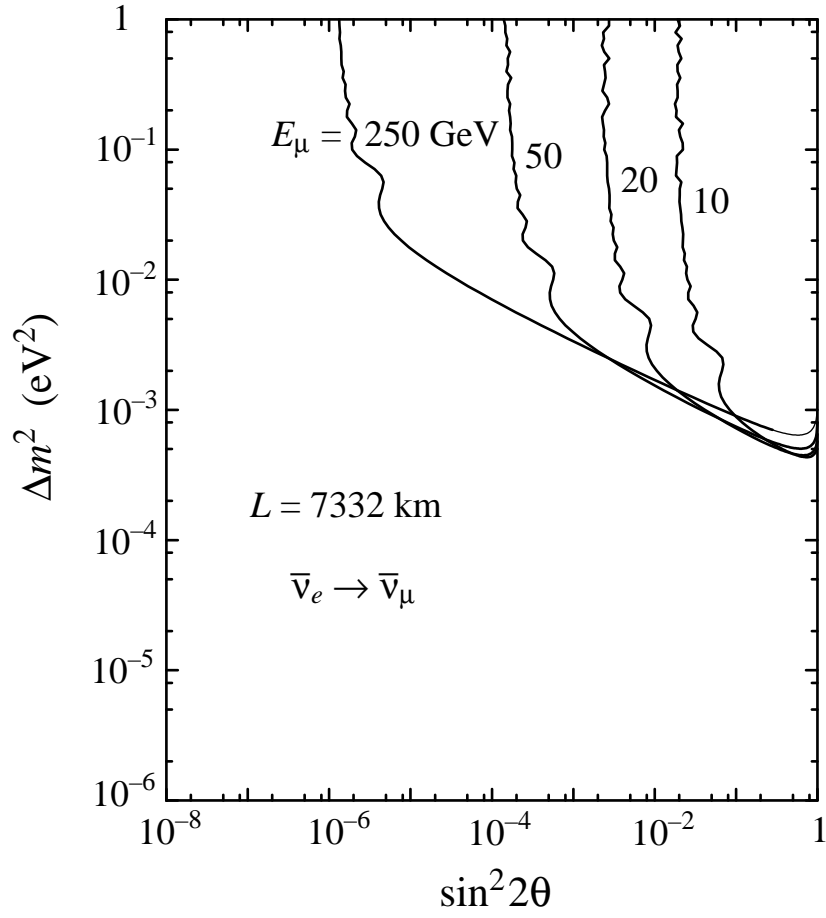


FIG. 19. (a) Single event per 10 kt-yr contours calculated for  $\bar{\nu}_e \rightarrow \bar{\nu}_\mu$  appearance 7332 km downstream of a muon storage ring neutrino source, assuming  $\Delta m^2 > 0$ . From left to right, the contours correspond to unpolarized muons with energies  $E_\mu = 250, 50, 20,$  and  $10$  GeV.

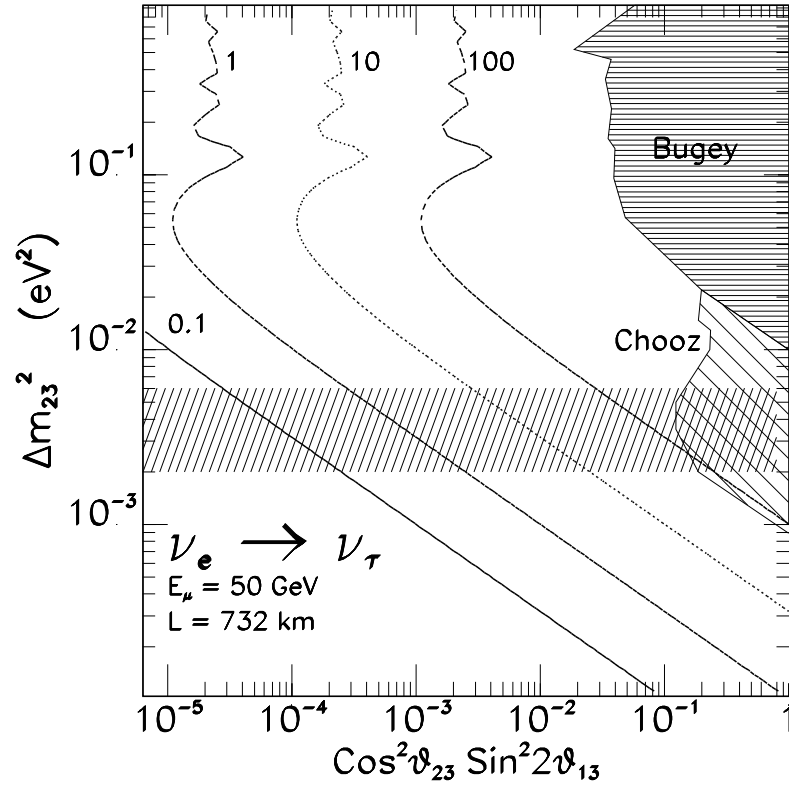


FIG. 20. Contours of constant  $\nu_\tau$  CC interaction event rate for  $\nu_e \rightarrow \nu_\tau$  appearance 732 km downstream of a 50 GeV muon storage ring neutrino source. From left to right, the contours correspond to event rates of 0.1, 1, 10, and 100 per kt-yr. The shaded areas are excluded by Bugey and Chooz  $\nu_e$  disappearance null results; the horizontal band indicates the range of  $\Delta m^2$  suggested by atmospheric neutrino oscillations.

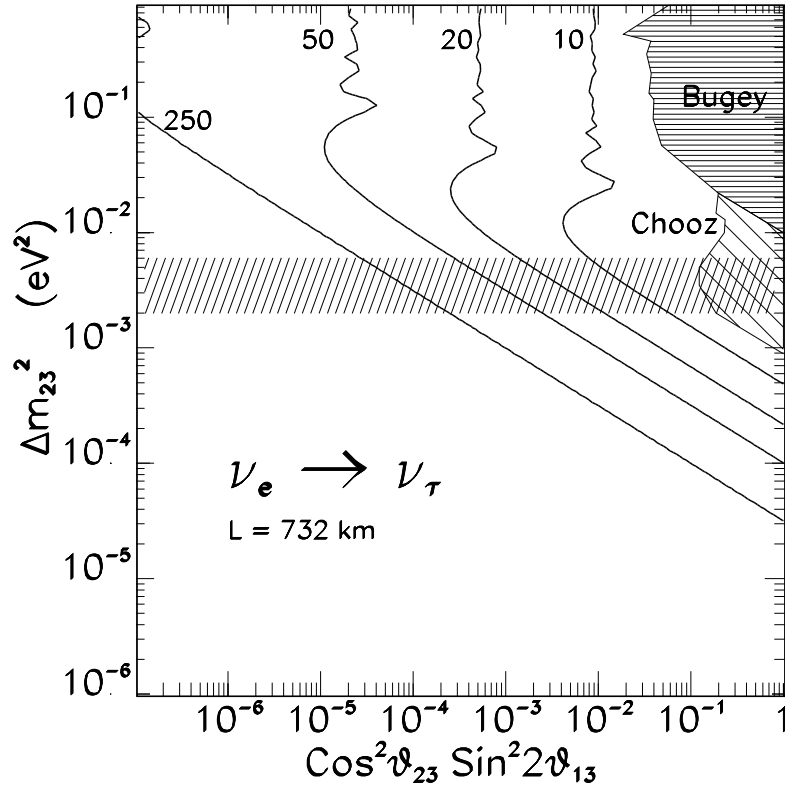


FIG. 21. Single event per kt-yr contours calculated for  $\nu_e \rightarrow \nu_\tau$  appearance 732 km downstream of a muon storage ring neutrino source. From left to right, the contours correspond to unpolarized muons with energies  $E_\mu = 250, 50, 20,$  and  $10 \text{ GeV}$ . The shaded areas are excluded by Bugey and Chooz  $\nu_e$  disappearance null results; the horizontal band indicates the range of  $\Delta m^2$  suggested by atmospheric neutrino oscillations.